modelling

MDPI

Article

A Study of Temperature and Humidity Conditions in a New Energy-Efficient Design of a Wall Structure with Air Gaps

Nurlan Zhangabay [1,*], Timur Tursunkululy [1], Akmaral Utelbayeva [2], Uliya Abdikerova [3,*] and Murat Sultanov [1]

[1] Department of Architecture and Urban Planning, M. Auezov South Kazakhstan University, Tauke Khan av., 5, Shymkent 160012, Kazakhstan; timurtursunkululy@gmail.com (T.T.); murat.sultanov@auezov.edu.kz (M.S.)
[2] Department of Chemistry, M. Auezov South Kazakhstan University, Tauke Khan av., 5, Shymkent 160012, Kazakhstan; mako_01-777@mail.ru
[3] Department of Architecture and Construction Production, Korkyt Ata Kyzylorda University, Saparbayev av., 15, Kyzylorda 120018, Kazakhstan
* Correspondence: nurlan.zhanabay777@mail.ru (N.Z.); abdikerova@korkyt.kz (U.A.)

Abstract: This manuscript presents a theoretical study of a newly developed energy-efficient external wall structure in comparison with a traditional ventilated facade. To conduct numerical studies based on mathematical models of the heat transfer of water vapor filtration through a multilayer filler structure with ventilated and non-ventilated air gaps, a calculation method was developed that additionally considers the presence of heat-reflecting screens and different variations in the geometric parameters of air gaps and thermal insulation layers. The study results demonstrated that the new energy-efficient multilayer wall structure was 6.1–7.2% more efficient in terms of heat transfer resistance than the traditional one, and due to the presence of heat-reflecting screens, the efficiency increased to 15.2–16.3% depending on the geometric parameters of the air and thermal insulation layers of the wall structure. In addition, in all the considered variants of the filler structure geometry (i.e., with closed and ventilated air gaps), there were water vapor condensation zones, but it was established that according to the value of the inadmissibility of moisture accumulation in multilayer wall structures, over the annual period of operation, the structures complied with the standard climatic conditions of Shymkent. The results of this study thus positively complement the existing catalog of energy-efficient wall structures, and the new wall structure can be used while considering the necessary geometric parameters of air and heat-insulating layers when designing buildings in the corresponding climatic conditions.

Keywords: thermophysical parameters; wall structure; air gaps; energy efficiency; mathematical model; calculation method

check for updates

Academic Editor: Wei Gao

Received: 13 January 2025
Revised: 28 January 2025
Accepted: 1 February 2025
Published: 5 February 2025

Citation: Zhangabay, N.; Tursunkululy, T.; Utelbayeva, A.; Abdikerova, U.; Sultanov, M. A Study of Temperature and Humidity Conditions in a New Energy-Efficient Design of a Wall Structure with Air Gaps. *Modelling* **2025**, *6*, 12. https://doi.org/10.3390/modelling6010012

Copyright: © 2025 by the authors. Licensee MDPI, Basel, Switzerland. This article is an open access article distributed under the terms and conditions of the Creative Commons Attribution (CC BY) license (https://creativecommons.org/licenses/by/4.0/).

1. Introduction

Energy conservation is an ongoing challenge for the world's scientific community, as it directly relates to environmental friendliness. In this regard, special attention is paid to this problem in various sectors of the economy, not least the construction industry, in which, according to the latest data [1], buildings consume about 30% of all final energy worldwide, with this figure exceeding 40% in the European Union [2]. One reason for this is that more than 80% of that energy is spent on heating buildings [3]. In connection with this problem, various strategies for modernizing residential buildings have been developed in many European countries to improve their energy efficiency [4]. Many studies are devoted to solving this problem, the results of which are used in the development of renovation programs both

at the private and state levels [5–7]. According to the European Directive on the Energy Performance of Buildings, a goal was set to reduce the amount of thermal energy consumed by 20% by 2020, compared to 1990 [8]. To achieve this goal, it was necessary to establish optimal energy efficiency requirements for new buildings and the modernization of existing buildings (replacement or repair of heating systems, air conditioning systems, wall thermal insulation, roof repair, etc.) [9]. Regarding the building structure, particular attention is given to outer-wall shells [10], responsible for up to 35% of all building energy losses [11]. To minimize this phenomenon, scientists and engineers are addressing various related problems, among which the use of air gaps in external wall structures has recently become popular, effective, and economically feasible [12–14]. To improve building energy efficiency, Santa Cruz, A.J. et al. [15] thus investigated the use of a ventilated facade with closed joints at different times of the year, in comparison with a traditional facade. Following the comparison of energy characteristics, the results showed that the presence of a ventilated facade increased the enclosure efficiency by more than 30%; however, the study was performed only in the presence of air gaps, and other enclosure design parameters were not measured. Liu L. et al. [16] conducted comprehensive studies on the energy-saving performance of a ventilated facade in hot and cold periods, studying the influence of the facade geometric parameters on the air flow rate. The results indicated that the ventilated facade exhibited an excellent energy-saving performance compared to a facade with a closed cavity. In addition, an appropriate facade configuration and air flow rate in the cavity were provided, with energy savings on the facade potentially reaching up to 90% in both summer and winter. To obtain satisfactory facade performance characteristics, the authors proposed maintaining an air velocity in the facade cavity in the range of 0.5–1 m/s. However, in their study, only the geometric parameters of the air gap were considered, and only the air flow rate was investigated. Nizovtsev M.I. et al. [17] conducted natural and laboratory studies on the effect of ventilated channels in a wall structure on the humidity of thermal insulation in cold periods. It was found that even with high room humidity (approximately 70%), the relative humidity of the air in the thermal insulation material did not exceed 50%, which demonstrated the high thermal insulation properties of the panels. In addition, a temperature stratification difference of up to 10 °C (with height) was recorded in the ventilated channels, which led to increased moisture removal from the thermal insulation. However, the study did not consider different variations in the geometric parameters of the air channels, which could have more clearly established the proposed design effectiveness. Gagliano A. et al. [18] conducted a comprehensive comparison of the thermal performance of an opaque ventilated facade and a conventional non-ventilated facade, considering two control days for the winter and summer periods. During their analysis, various facade orientations were studied, and two airiness states were considered: a state of calm wind, and a state with a wind speed above zero (i.e., 5.0 m/s at a height of 10 m). The results of the study showed that the opaque ventilated facade delivered energy savings in the range of 20 to 55%, with the highest indicator observed on a summer day on the facade facing east/west. However, according to the authors of another study [11], their results would positively complement those of a variation analysis of ventilated layer geometry. In a numerical study, Borodulin V.Y. et al. [19] developed a physical and mathematical model of a brick wall insulated with panels with ventilated channels. The comparative calculation results showed that for a sharply continental climate, two characteristic peaks in relative moisture content were observed in the panel's thermal insulation material: one peak corresponded to the end of summer/beginning of autumn, while the second corresponded to winter/beginning of spring. In addition, these studies were conducted without performing a variation analysis of geometric parameters with the use of a heat-reflecting coating, which, according to the results of the authors' modeling, would significantly increase the struc-

ture's thermal characteristics [20,21]. This was also established in [22], where, for example, an increase in the air cavity to 110 mm increased the heat flow up to 1.5 times, and the use of reflective thermal insulation contributed to a change in temperature of up to 30% [23]. Hassan K.A. et al. [24] investigated the effect of closed air gaps in double walls on the thermal insulation properties of an enclosure. Six models of double walls with gaps up to 6 cm thick were experimentally investigated, yielding the following results: an increase in the gap thickness led to an asymptotic increase in the thermal resistance of the enclosure, and the optimal gap thickness was 6 cm, which reduced heat loss by almost 20% compared to a 1 cm gap. The effectiveness of the ventilated facade was also confirmed in [25], where it was found that the condensation zone shifted to the outer thermal insulation layer, which bordered the ventilated air gap. In other research, the thermal insulation location on the outside helped to increase the heat-accumulating capacity of the wall massif [26,27]. Similarly, the efficiency performance of applying facades with air gaps was also studied in the climatic conditions of China, where the correct facade configuration facilitated a reduction in energy consumption by 11.4% and 6.5% compared to a conventional monolithic facade, respectively [28]. A study [29] on the use of closed air channels in parallel with a ventilated air layer proved the importance and effectiveness of these design solutions, and the authors recommended conducting further versatile and variable studies to determine the most effective geometric parameters. Additionally, to verify the reliability of the results obtained via modeling using the ANSYS-19.2 software package, the authors decided to conduct further numerical studies. Summaries of the cited studies and their respective relationship with the current study are presented in Table 1.

In this regard, at this stage, the authors of this study set the task of investigating a new energy-efficient wall structure of an external fence, whereby, based on the developed mathematical model, a new numerical method for calculating a multilayer energy-efficient wall structure is compiled, considering ventilated and enclosed air layers, as well as a heat-reflecting screen located in the thermal insulation layer of the structure. The presence of these structural solutions as part of a single multilayer fence represents an innovative solution, confirming the effectiveness required by a comprehensive multi-stage study, whereby previous studies (by the same authors) on this wall structure have shown significant effectiveness, being conducted using the ANSYS software package [20] and via reduced model experiments under laboratory conditions [29]. At this stage, the authors propose a variable study of a new structure with different geometric parameters based on a numerical methodology. The aim is to confirm the results of previous studies and establish the most effective design solutions, where the results of the study will positively complement the existing catalog of exterior wall structures and the current methods for calculating energy-efficient facades, as indicated in the works given in Table 1. This study also aims to provide a more accurate understanding of effective design solutions for and geometric parameters of ventilated and enclosed air layers, with the implementation of a heat-reflecting screen.

Table 1. Summaries of cited studies and their relationship with the current study.

Research	Research Time	The Relationship with the Current Study
[12]	2023	A review of the study confirms that there is no single definition, design, or configuration of a double-faced facade, and there are many assessment methods that depend on the changing climate, geometry, construction applications, and materials.

Table 1. *Cont.*

Research	Research Time	The Relationship with the Current Study
[13]	2016	The study is intended for countries with a temperate climate, which corresponds to most of the Republic of Kazakhstan. In addition, in the study, key parameters of the facade were taken as criteria, such as the configuration of the facade, the width of the cavity and ventilation, and the parameters of the building in the form of orientation and climate zone.
[14,20,21,29]	2023	The study is part of a comprehensive study by the authors on the development of new energy-efficient facades for the territories of the Republic of Kazakhstan, which were conducted based on the modeling method in the ANSYS software package, which confirms the significant contribution of the authors to the development of this scientific field.
[15]	2017	The study was conducted based on the use of double air layers with a comparative analysis of traditional facades with a ventilated layer.
[16,25,27]	2017, 2016, 2015	The influence of the configuration of materials in a ventilated facade and the air flow velocity in the cavity on the thermal characteristics of the facade was studied.
[17]	2020	Field-experiment-based study on new facade systems with ventilated channels to remove excess moisture from the insulating material. The influence of ventilated channels in facade panels on the moisture state of thermal insulation was studied.
[18]	2020	The study offers a comprehensive comparison of the thermal characteristics of an opaque ventilated facade and a conventional non-ventilated facade, considering two control days for winter and summer periods. During the analysis, the influence of the facade location was studied, and windiness was considered.
[19]	2021	The study examined the thermal and moisture conditions of a brick wall of a building insulated with panels with ventilated channels in a long-term operation cycle. A new physico-mathematical model was also developed for calculating heat and moisture transfer processes in facades with such panels.
[22,23]	2022	The influence of the flow behavior in a naturally ventilated cavity on the operational characteristics of light and heavy wall structures with traditional passive and active facades was investigated.
[24,28]	2022	The improvement of the thermal characteristics of building wall enclosures was investigated by constructing hollow (double) walls and determining the optimal thickness of the air gap between the walls used as thermal insulation to improve or reduce heat transfer.
[26]	2020	The use of interactive solutions in the construction of exterior wall fences.

2. Methods and Materials

2.1. Initial Data for Modeling

By way of comparison, we considered three filler structure schemes:

Option 1: a multilayer wall filler structure with homogeneous bearing and heat-insulating layers and with a closed ventilated air gap (Figure 1a).
Option 2: a multilayer wall filler structure with homogeneous bearing and heat-insulating layers and closed and ventilated air gaps without a heat-reflecting coating (Figure 1b).
Option 3: a multilayer wall filler structure with homogeneous bearing and heat-insulating layers and closed and ventilated air gaps with a heat-reflecting coating, which is applied to the external side of the closed air gap (Figure 1c).

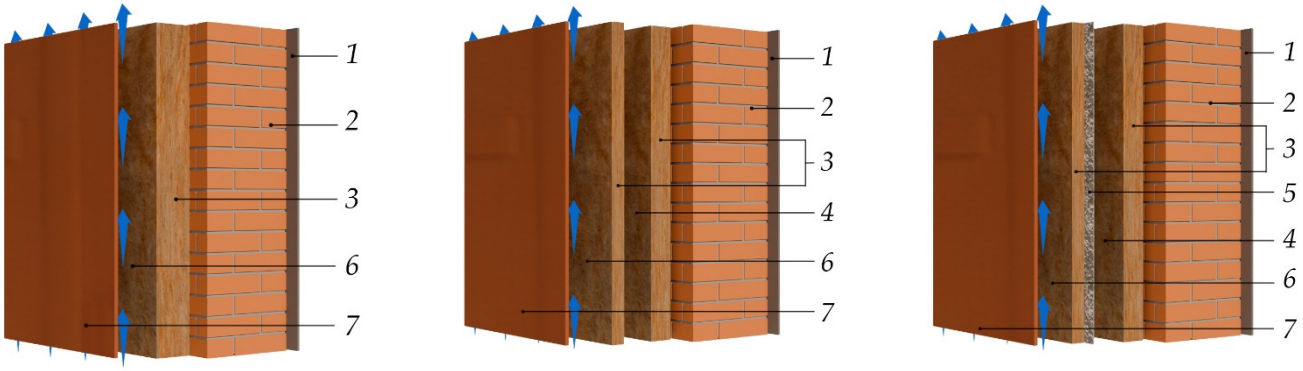


Figure 1. Multilayer wall filler structures: (**a**) Option 1, (**b**) Option 2, and (**c**) Option 3, with the following layer fillers: 1. cement–sand plaster, 2. ceramic brick laying, 3. extruded cellular polystyrene, 4. closed air gap, 5. heat-reflecting coating, 6. ventilated air gap, and 7. ceramic granite.

We assumed that there was an ideal level of thermal contact between the layers of filler structures. In the calculations, we neglected the thickness of heat-reflecting coatings, and considered the coating itself as a gray body [30–33] with a given absorption coefficient. Such assumptions did not introduce significant errors into the calculation results due to the insignificance of the thermal resistance of non-ideal thermal contact, which occurs in reality, as well as the small thickness and high thermal conductivity of the heat-reflecting coating [30–33]. In addition, these assumptions made the calculation model universal in relation to the presence/absence of a heat-reflecting coating: if we set its absorption coefficient equal to the absorption coefficient of the layer on which it is applied, we will obtain a calculation model corresponding to the filler structure scheme without this heat-reflecting coating.

The thermal characteristics of the specified structure layers are given in Table 2. It should be noted that these parameters were selected primarily because, all other things being equal, various methods of insulating the bearing structure could then be investigated. In this regard, issues regarding the technical feasibility of these schemes were not considered. For example, in all three schemes, the facing layer is considered a flat body in contact with a ventilated air gap, without specifying how it is attached to the bearing layer of the filler structure.

Table 2. Characteristics of the filler structure layers according to Figure 1.

Layer Number	Description	Thickness, mm	Density, kg/m^3	Thermal Conductivity Coefficient, W/(m·°C)	Vapor Permeability, mg/(m·h·Pa)
1	Cement–sand plaster	10	1800	0.76	0.09
2	Ceramic brick laying	380	1400	0.58	0.14
3	Extruded cellular polystyrene	As per Table 2	25	0.03	0.005
4	Closed air gap	As per Table 2	-	-	-
5	Heat-reflecting coating	-	-	-	-
6	Ventilated air gap	As per Table 2	-	-	-
7	Ceramic granite	10	2800	3.49	0.008

Option 3 assumes the use of heat-reflecting coatings made of aluminum foil, which can be applied to the outer wall of the closed air gap (i.e., to the internal surface of the extruded cellular polystyrene layer, number 5). The emissivity factor of the surfaces limiting the air gaps and air channels in the extruded cellular polystyrene with and without a heat-reflecting coating was taken as 0.039 and 0.9, respectively.

A comparison of the filler structures under consideration was performed under the conditions of a steady-state temperature regime with an inside air temperature of 21 °C and

an outside air temperature of −14.3 °C, which corresponds to the coldest five-day period with a probability of 0.92 in the conditions of the climatic zone of Shymkent, Republic of Kazakhstan [34,35]. The heat transfer coefficients on the internal and external surfaces of the filler structure were taken to be 8.7 and 23 W/(m^2·°C), respectively, according to [36].

According to the problem statement, at the considered temperature in the room, the relative air humidity was 50–60%. The theory and practice of calculating filler structures show that transient thermal conditions caused by changes in internal and external thermal effects on the filler structure can last up to several days after the internal and external effects cease to change. This is due to the significant thermal inertia properties of filler structures (primarily their bearing layers). During this period of days, the actual air parameters inside and outside the room undergo changes caused primarily by daily fluctuations in atmospheric air parameters and the daily periodicity of room use. The established stationary mode, which is usually considered in building thermal physics, is thus nothing more than an averaging of the thermal physical parameters over several days (temperature, humidity, etc.) at each point of the filler structure. All initial data must, therefore, be taken as averages for a given period. For example, for this reason, the average outside air temperature for the coldest five-day period was considered, and not the minimum air temperature in the coldest month. We did the same with humidity. For comparative calculations, the average value from the humidity range was used, i.e., a relative humidity in the room of 55% was assumed. We also took the average relative humidity of the outside air as averaged, i.e., the average for the coldest month. According to [34], the average for the coldest month (January) was 73%. We assumed the difference in height between the supply and exhaust openings of the ventilated air gap to be equal to the height of the building facade, namely, 18 m. We also took the sum of local resistances to be 5.4.

To perform the comparative calculations, we selected some geometric parameters of the filler structures under consideration, namely, the thickness of the ventilated and closed air gaps, as per Table 3.

Table 3. Considered options of geometric parameters of filler structures.

No.	Performance of Filler Structure	Thickness of Ventilated Air Gap, mm	Thickness of Closed Air Gap, mm	Thickness of the Thermal Insulation Layer Made of Solid Extruded Cellular Polystyrene, mm	Designation
1	Option 1	200	-	80 (layer 3)	Option 1
2	Option 2, 3	175 (layer 6)	25 (layer 4)	30/50 (layer 3)	Option 2, 3/175/25
		150 (layer 6)	50 (layer 4)	30/50 (layer 3)	Option 2, 3/150/50
		125 (layer 6)	75 (layer 4)	30/50 (layer 3)	Option 2, 3/125/75
		100 (layer 6)	100 (layer 4)	30/50 (layer 3)	Option 2, 3/100/100
		75 (layer 6)	125 (layer 4)	30/50 (layer 3)	Option 2, 3/75/125
		50 (layer 6)	150 (layer 4)	30/50 (layer 3)	Option 2, 3/50/150
		25 (layer 6)	175 (layer 4)	30/50 (layer 3)	Option 2, 3/25/175

As a determining parameter for comparison, we considered heat transfer resistance—the higher it is, the higher the heat-protective properties of a given filler structure. In addition, options in which there may be zones of water vapor condensation inside the filler structure were rejected.

According to heat transfer theory [32,37–41], it is known that the heat transfer resistance for the simplest case of a filler structure, in the form of a multilayer wall with homogeneous layers, is defined as:

$$R = \frac{1}{\alpha_{\text{int}}} + \sum_{i=1}^{n} \frac{\delta_i}{\lambda_i} + \frac{1}{\alpha_{ext}}. \quad (1)$$

Equation (1) does not facilitate adequate consideration of the radiant component of heat transfer between the walls that limits the air gaps. The method of determining the reduced heat transfer resistance will, therefore, be based on the calculation of temperature fields according to [37]. When using this method, we assume that the filler structures under consideration are homogeneous in the vertical direction, i.e., neither the temperature nor the heat flow depend on the corresponding coordinate.

According to [36,37,41], the reduced heat transfer resistance in this case is calculated using the formula:

$$R = (T_{int} - T_{ext})A/Q. \quad (2)$$

2.2. Development of a Mathematical Model of Heat Transfer Through a Multilayer Filler Structure with Ventilated and Non-Ventilated Air Gaps

In constructing a mathematical model of heat transfer through the filler structures under consideration, we introduced an additional assumption to those stated above: in a closed air gap (Options 2 and 3), according to [30,31], a detailed mathematical model of convective heat exchange in a moving medium containing the continuity equation, the Navier–Stokes motion equations, and the energy equation will not be considered. Instead, these layers will be described as a homogeneous isotropic body with equivalent thermal conductivity, which considers conductive, convective, and radiant components of heat transfer through the filler structure layer under consideration.

As changing the temperature in each layer does not lead to significant changes in thermal conductivity, the problem can thus be considered in a linear formulation.

The described assumptions allow the problem of heat transfer (through any of the investigated filler structures) to be considered in a one-dimensional stationary statement.

We directed the spatial axis x in the direction from the room to the outside, placing the origin on the internal filler structure surface. Introducing the designation δ_i for the thickness of the i-th layer of the filler structure, the following expressions can then be written:

$$x_0 = 0, \quad (3)$$

$$x_k = \sum_{i=1}^{k} \delta_i, \quad (4)$$

$$x_n = \sum_{i=1}^{n} \delta_i. \quad (5)$$

For each layer, except for the ventilated air gap, a one-dimensional linear, stationary thermal conductivity equation can be written:

$$\lambda_k \frac{\partial^2 T}{\partial x^2} = 0, \quad x_{k-1} < x < x_k, \quad k = 1, \ldots n. \quad (6)$$

At the junction of the layers, due to ideal thermal contact, the relationships describing the equality of temperature and heat flow are fulfilled:

$$T|_{x=x_k-0} = T|_{x=x_k+0}, \quad k = 1, \ldots n-1, \quad (7)$$

$$\lambda_k \left.\frac{\partial T}{\partial x}\right|_{x=x_k-0} = \lambda_{k+1} \left.\frac{\partial T}{\partial x}\right|_{x=x_k+0}, \quad k = 1, \ldots n-1. \quad (8)$$

The convective heat exchange of the filler structure with the surrounding air environment is described by the following boundary conditions:

On the internal filler structure surface:

$$\lambda_1 \left.\frac{\partial T}{\partial x}\right|_{x=0} = \alpha_{\text{int}}(\,T|_{x=0} - T_{\text{int}}). \tag{9}$$

On the external filler structure surface:

$$\lambda_n \left.\frac{\partial T}{\partial x}\right|_{x=x_n} = \alpha_{ext}\Big(\,T|_{x=x_n} - T_{ext}\Big). \tag{10}$$

To simplify subsequent entries, we introduced the following designations:

$T_0 = T(0)$: temperature on the internal filler structure surface,
$T_k = T(x_k)$: temperature at the junction of layers with numbers x_k and x_{k+1},
$T_n = T(x_n)$: temperature on the external filler structure surface.

Thermal conductivity coefficients for layers without air gaps were specified based on the initial data of Table 1.

For a layer consisting entirely of a closed air gap (layer $k = 4$ in Option 2), in Equation (6), it is necessary to use the equivalent thermal conductivity value λe. We denoted it as λ_{eq}.

When introducing equivalent thermal conductivity, a homogeneous isotropic body was considered, and its heat flow density in the x direction can thus be written as follows:

$$q = -\lambda_{eq}\frac{\partial T}{\partial x}. \tag{11}$$

Due to the one-dimensionality of the problem and the absence of internal heat sources, the partial derivative of the temperature with respect to the spatial coordinate in Equation (11) could be accurately written as a finite difference, which allowed us to rewrite (11) as follows:

$$q = -\lambda_{eq}\frac{T_k - T_{k-1}}{\delta_k} = \lambda_{eq}\frac{T_{k-1} - T_k}{\delta_k}. \tag{12}$$

On the other hand, when considering an air gap, the heat flow can be represented as the sum of two components—conductive–convective and radiant:

$$q = q_c + q_r. \tag{13}$$

According to [31], in vertical air gaps between flat walls, conductive–convective heat transfer during natural convection can be adequately described by mathematical models for stationary layers, using the concept of the effective thermal conductivity coefficient λ_K, which is defined as follows:

$$\begin{gathered} \lambda_e = \lambda_t \quad \text{at} \quad \text{Ra} < 104, \\ \lambda_e = \lambda_t \cdot 0.062 \cdot \text{Ra}^{1/3} \quad \text{at} \quad 10^4 < \text{Ra} < 10^4, \\ \lambda_e = \lambda_t \cdot 0.22 \cdot \text{Ra}^{1/4} \quad \text{at} \quad 10^7 < \text{Ra} < 10^{10}, \end{gathered} \tag{14}$$

where $\text{Ra} = \frac{g\delta^3\beta\Delta T}{\nu} Pr$.

The values λ_t, ν, and Pr, when using Equation (14), are taken at average values of temperature and pressure in the air gap.

Thus,

$$q_c = \lambda_e\frac{\partial T}{\partial x}. \tag{15}$$

The density of the radiant heat flow component according to [30–32] can be found from the expression:

$$q_r = \varepsilon\sigma_0({T_{k-1}}^4 - {T^4}_k). \tag{16}$$

Substituting (12), (15), and (16) into (13) and using for (15) the same finite-difference notation of the partial derivative of temperature as in (12), we obtained:

$$\lambda_{eq}\frac{T_{k-1}-T_k}{\delta_k}=\lambda_e\frac{T_{k-1}-T_k}{\delta_k}+\varepsilon\sigma_0\left(T_{k-1}^4-T_k^4\right), \tag{17}$$

from which we have:

$$\lambda_{eq}=\lambda_e+\frac{\delta_k\varepsilon\sigma_0\left(T_{k-1}^4-T_k^4\right)\ \delta_k}{T_{k-1}-T_k}. \tag{18}$$

To create a mathematical model of heat exchange in a ventilated air gap, we used the energy equation, which in the general multidimensional non-stationary case can be written as:

$$c\rho\frac{dT}{d\tau}=\lambda\Delta T+q_V. \tag{19}$$

In the ventilated air gap, a clearly defined upward air flow was formed with no local vortices. In addition, due to the insignificance of viscous effects in the boundary layers near the walls limiting the gap, it can be assumed that the air velocity was constant in the cross-section of the gap. In addition, since the air temperature changed insignificantly as it moved in the gap, it was possible to neglect the air compressibility in the energy equation and assume that its density remained constant. As the air flow rate was a constant value, we then ascertained that the air velocity could be taken as a constant at each point of the ventilated gap. In this case, by representing in (19) the total time derivative through partial time derivatives, it was possible to write a one-dimensional stationary version of this equation:

$$c\rho v\frac{\partial T}{\partial z}=\lambda\frac{\partial^2 T}{\partial z^2}+q_V. \tag{20}$$

We wrote the volumetric density of internal heat sources based on the heat balance of flows passing through the walls that limit the gap: the amount of heat entering the elementary volume of air in the gap was equal to the difference between the amount of heat entering the gap from the room and the amount of heat removed through the external facing into the surrounding space:

$$\delta Q_V=\delta Q_{int}-\delta Q_{ext}. \tag{21}$$

For an elementary volume of $\delta_k \times \delta L \times \delta z$ size (δ_k is the gap thickness, while δL and δz are the extents of the elementary volume in the horizontal and vertical directions, respectively), (21) can be written as:

$$q_V\cdot\delta_k\cdot\delta L\cdot\delta z=\alpha_{\text{п}}\cdot\delta L\cdot\delta z\,(T_{k-1}-T(z))-\alpha_{\text{п}}\cdot\delta L\cdot\delta z\,(T(z)-T_k). \tag{22}$$

From Equation (22), we obtained an expression for the specific volumetric density of internal heat sources:

$$q_v=\frac{\alpha_a}{\delta_k}(T_{k-1}+T_k-2T(z)). \tag{23}$$

In the mathematical model under consideration, since the air velocity in the ventilated air gap remained constant with the change in height, and the temperature of the walls limiting the gap was assumed to be constant, it can be assumed that, by virtue of (22), the air in the gap was heated equally at each of its points. Consequently, the dependence $T(z)$ is a linear function of the vertical coordinate. The second derivative, with respect to

the vertical coordinate of the air temperature in the gap, was thus equal to zero, and by considering (23), (20) can be rewritten as:

$$cpv = \frac{dT}{dz} = \frac{\alpha_a}{\delta_k}(T_{k-1} + T_k - 2T(z)). \quad (24)$$

The initial condition for Equation (24) was determined based on the fact that at the lowest point of the air gap, there was an air flow, and its temperature was equal to the atmospheric air temperature:

$$T(0) = T_{ext}. \quad (25)$$

The value of the heat transfer coefficient $\alpha_п$ was obtained from the known criteria equations for a flat channel [30–32]:

$$\text{Nu} = \text{Nu}(\text{Re}, \text{Pr}), \quad (26)$$

where $\text{Nu} = \alpha_a/(\delta_k \cdot \lambda)$.

The solution of the ordinary differential Equation (24) with the initial condition (25) had the form:

$$T(z) = \left[T_{\text{ext}} - \frac{T_{k+1} + T_k}{2}\right] \cdot \exp\left(-\frac{2\alpha_a}{\delta_k c\rho v} z\right) + \frac{T_{k+1} + T_k}{2}. \quad (27)$$

The average air temperature in the ventilated gap was found as the average integral value over the height:

$$T_п = \frac{1}{H}\int_0^H T(z)dz = \frac{1}{H}\left[1 - \frac{T_{\text{ext}} - \frac{T_{k+1} + T_k}{2}}{2\alpha_a}\delta_k c\rho v \cdot \exp\left(-\frac{2\alpha_a}{\delta_k c\rho v} H\right)\right]. \quad (28)$$

The air temperature at the exit of the ventilated gap was obtained from Equation (27) at $z = H$:

$$T_{\text{out}} = \left[T_{\text{ext}} - \frac{T_{k+1} + T_k}{2}\right] \cdot \exp\left(-\frac{2\alpha_a}{\delta_k c\rho v} H\right) + \frac{T_{k+1} + T_k}{2}. \quad (29)$$

The air velocity in the ventilated air gap was found based on the equality of the total pressure losses in the ventilated air gap and the driving pressure (stack effect), which is caused by the Archimedes forces arising due to the difference in the air density in the ventilated air gap and at the exit from it:

$$\Delta p^{\text{o}} = p_{\text{c}}. \quad (30)$$

Neglecting the pressure losses in the supply and exhaust pressures (Equation (30)) in the case of a flat vertical slotted channel, we can rewrite it as:

$$\xi(H/2\delta_k)\rho_a v^2/2 = (\rho_{\text{ext}} - \rho_{\text{out}})gH. \quad (31)$$

The air density at a given temperature in (31) can be obtained from the Clapeyron–Mendeleev equation:

$$\rho_i = p_i/(RT_i), \quad (32)$$

in which the pressure of 1 atm can be taken as the thermodynamic pressure p_i.

The balance of heat flows in the gap is described by the energy conservation law: the amount of heat entering the ventilated air gap from the room Q_{int} is equal to the sum of the amount of heat carried away by the ventilation air Q_{out}, the amount of heat transferred via

convection from the air gap to the external facing Q_{ext}, and the amount of heat transferred via radiant heat exchange from the internal wall of the gap to the external wall $Q_{\text{л}}$:

$$Q_{\text{int}} = Q_{\text{out}} + Q_{\text{ext}} + Q_r. \tag{33}$$

For a unit length of the filler structure in the horizontal direction δL, these values can be written as:

$$Q_{\text{int}} = \alpha_{\text{п}}(T_{k-1} - T_{\text{п}})\cdot H\cdot\delta L, \tag{34}$$

$$Q_{\text{ext}} = \alpha_{\text{п}}(T_{\text{п}} - T_k)\cdot H\cdot\delta L, \tag{35}$$

$$Q_{\text{out}} = v\ \rho\cdot\delta_k\cdot\delta L\cdot c\cdot(T_{\text{out}} - T_{\text{ext}}), \tag{36}$$

$$Q_r = \varepsilon\cdot\sigma_0\cdot({T_{k-1}}^4 - {T_k}^4)\cdot H\cdot\delta L, \tag{37}$$

where ε is the reduced emissivity factor of the gap walls, which in the case of two flat parallel walls of great length can be calculated according to the expression $\frac{1}{\varepsilon} = \frac{1}{\varepsilon_{k-1}} + \frac{1}{\varepsilon_k} - 1$.

Substituting (34)–(37) into (33), we obtained:

$$\alpha_a(T_{k-1} - T_a)\cdot H = \alpha_a(T_a - T_k)\cdot H + v\ \rho\cdot\delta_k\cdot c\cdot(T_{\text{out}} - T_{\text{ext}}) + \varepsilon\cdot\sigma_0\cdot({T_{k-1}}^4 - {T_k}^4)\cdot H. \tag{38}$$

The mathematical model of the phenomenon of heat transfer through the filler structure is thus described using the following set of equations:

1. For all layers except the ventilated air gap, the heat flow was determined as in (12). In this case, either the corresponding thermophysical characteristic of the material (in the case of a solid layer) or the equivalent value of the thermal conductivity coefficient calculated using Equation (18) was used as the thermal conductivity coefficient in (12).
2. Equations (28), (29), (31), (32), and (38) were used for the ventilated air gap.
3. Boundary conditions (9) and (10) were used.

This mathematical model allowed us to determine the temperature distribution T_k at the junction of layers, the air temperature in the ventilated air gap $T_{\text{п}}$ and at its exit T_{out}, and the air velocity in the ventilated air gap v. The temperature inside each layer was found following the linear approximation of temperatures T_k.

2.3. Development of a Mathematical Model for Water Vapor Filtration Through a Multilayer Filler Structure with Ventilated and Non-Ventilated Air Gaps

The mathematical model of vapor filtration through the filler structure is based on Darcy's law [42], which in the one-dimensional case can be written as:

$$q_{vp} = \mu\frac{\partial e}{\partial x}. \tag{39}$$

Within one homogeneous layer of the filler structure, the dependence of the vapor permeability coefficient on temperature can be neglected due to the relatively small range of temperature changes and is considered a constant. In this case, the direct integration of Equation (39) over the layer thickness allowed us to write the following relationship:

$$\Delta e = e_{k-1} - e_k = q_{vp}\cdot\frac{\delta_k}{\mu_k}. \tag{40}$$

Equation (40) can be rewritten as:

$$q_{vp} = \frac{e_{k-1} - e_k}{R_{vp\,i}}, \tag{41}$$

where $R_{vp\,k} = \delta_k / \mu_k$ represents the vapor permeability resistance of the layer under consideration.

Similar expressions can be used for a closed air gap. Heating from its warmer internal wall, the air expands and rises due to the Archimedes forces. Near the opposite cold wall, it cools and descends. As a result, a circulation flow of air is formed inside the closed air gap in the form of one large vortex or several individual vortices located one above the other [32]. The number of vortices depends on the temperature difference on the opposite walls and on the geometric dimensions of the gap, but, in any case, they contribute to the mixing of air inside it, including water vapor in the air. Equally, as the temperature differences are small, these flows do not lead to significant changes in the distribution of air pressure over the gap volume. In this mathematical model, it can, therefore, be considered that the air pressure, and accordingly the partial pressure of water vapor within the gap, is a constant value. If the temperature difference is so small that convective flow in the gap does not form, then the assumption of constant partial pressure is also valid due to the Brownian motion of molecules, which also guarantees the mixing of air components. In any case, for the closed air gap, it can be concluded that the partial pressure of water vapor of the air of the internal and external walls is the same. As a result, in Equation (40),

$$e_{k-1} = e_k, \tag{42}$$

which corresponds to an infinitely large "vapor permeability coefficient" of air, and zero "vapor permeability resistance" of the air gap.

The introduction of these two conventional values (given in quotation marks) facilitates the formation of a uniform mathematical model of vapor permeability for both solid layers and air gaps. This approach is convenient for the formation of a general mathematical model for the entire filler structure and for simplifying the methodology for its calculation.

Since the temperature and humidity conditions of the structures under study were considered in a stationary one-dimensional formulation, the q_{vp} value remained constant within the part of the filler structure from the room to the ventilated air gap. In this case, combining expressions of the type (41), written for each layer and for this entire part of the structure, the following relationship was obtained:

$$q_{vp} = \frac{e_{\text{int}} - e_a}{R_{vp\text{int}}}, \tag{43}$$

where $R_{vp\ \text{int}}$ represents the vapor permeability resistance of the multilayer structure, which can be calculated as:

$$R_{vp\,\text{int}} = \sum_{i=1}^{n_{\text{int}}} R_{vp\ i} = \sum_{i=1}^{n_{\text{int}}} \frac{\delta_i}{\mu_i}. \tag{44}$$

We constructed a mathematical model of vapor transfer in a ventilated air gap based on the mass conservation law: the amount of water vapor entering the ventilated air gap through the wall from the room, $Q_{vp\ \text{int}}$, was equal to the sum of the amount of water vapor leaving the ventilated water gap through the external facing, $Q_{vp\ \text{ext}}$, and the amount of water vapor carried away by the ventilation air passing through the gap. For an elementary volume of air in the gap occupying its entire thickness δ_k and having a height dz and a horizontal dimension along the filler structure dL, these values were represented as:

$$dQ_{vp\ int} = q_{vp\ int} \cdot dz \cdot dL, \tag{45}$$

$$dQ_{vp\ ext} = q_{vp\ ext} \cdot dz \cdot dL, \tag{46}$$

$$dQ_{vp\,\text{out}} = \frac{m(z+dz) - m(z)}{d\tau} = dL \cdot dz \cdot \delta_k \frac{\rho(z+dz) - \rho(z)}{d\tau}. \tag{47}$$

It is obvious that

$$dz = v \cdot d\tau. \tag{48}$$

According to Bernoulli's law, considering the previously made assumption about the constancy of the air velocity in the ventilated air gap by height, the following relationship was written:

$$\frac{\rho(z+dz)\cdot v^2}{2} + e(z+dz) = \frac{\rho(z)\cdot v^2}{2} + e(z). \tag{49}$$

Combining (45)–(47) by considering (48) and (49), we obtained:

$$q_{vp\,\mathrm{int}} \cdot dz \cdot dL = q_{vp\,\mathrm{ext}} \cdot dz \cdot dL + dL \cdot dz \cdot \delta_k \cdot \frac{2}{v^2} \cdot \frac{e(z+dz) - e(z)}{dz} \cdot v, \tag{50}$$

or

$$q_{vp\,\mathrm{int}} = q_{vp\,\mathrm{ext}} + \delta_k \cdot \frac{2}{v} \cdot \frac{e(z+dz) - e(z)}{dz}. \tag{51}$$

Passing to the limit $dz \to 0$ in (51), we obtained an ordinary first-order differential equation describing the distribution of the water vapor partial pressure in the ventilated gap:

$$\frac{de}{dz} = \left(q_{vp\,\mathrm{int}} - q_{vp\,\mathrm{ext}}\right)\frac{v}{2\delta_k}. \tag{52}$$

We wrote the initial condition for Equation (51) based on the fact that at the entrance to the ventilated air gap, the vapor partial pressure was equal to the atmospheric air partial pressure:

$$e(0) = e_{\mathrm{ext}}. \tag{53}$$

Considering the assumption made at the beginning of the construction of the mathematical model about the one-dimensionality of the problem, the $q_{vp\ \mathrm{int}}$ and $q_{vp\ \mathrm{ext}}$ values were constants. The solution of (52) and (53) can, therefore, be written as:

$$e(z) = \left(q_{vp\,\mathrm{int}} - q_{vp\,\mathrm{ext}}\right)\frac{v}{2\delta_k}z + e_{\mathrm{ext}}. \tag{54}$$

Equation (54) allowed us to determine the water vapor partial pressure at the exit of the ventilated air gap e_{out} and the average height value of the water vapor partial pressure in the ventilated air gap:

$$e_{\mathrm{out}} = e(H) = \left(q_{vp\,\mathrm{int}} - q_{vp\,\mathrm{ext}}\right)\frac{v}{2\delta_k}H + e_{\mathrm{ext}}, \tag{55}$$

$$e_a = e(H) = \left(q_{vp\,\mathrm{int}} - q_{vp\,\mathrm{ext}}\right)\frac{v}{4\delta_k}H + e_{\mathrm{ext}}. \tag{56}$$

Note that in this mathematical model of the water vapor transfer in the ventilated mathematical gap, as in the case of the closed air gap, it was assumed that due to the mixing of air caused by the Brownian motion of molecules, the water vapor partial pressure remained unchanged across the gap thickness. That is,

$$e_a = e_{k-1} = e_k. \tag{57}$$

The mathematical model of the water vapor filtration through the considered multilayer filler structures is thus described using the following equations:

1. For each layer, except for the ventilated air gap, the water vapor flow was determined as in (41). The same relationship was valid for the external facing. In this case, for the closed air gap, Equation (42) was used.

2. The set of layers from the room to the ventilated air gap was described by Equations (43) and (44).
3. In the ventilated air gap, Equations (55)–(57) were used.
4. The boundary conditions were taken to be the values of the water vapor partial pressure on the internal and external surfaces of the filler structure, corresponding to the water vapor partial pressures indoors and outside:

$$e_0 = e_{\text{int}}, \tag{58}$$

$$e_n = e_{\text{ext}}. \tag{59}$$

2.4. Development of a Methodology for Calculating Temperature Fields and Humidity Conditions in the Filler Structures Under Consideration

For calculations using the mathematical model described in the previous section, we used the iteration procedure. As key parameters were updated at each iteration, we considered the temperature and partial pressure of the water vapor on the internal and external surfaces of the filler structure and at the junction of layers: T_k, e_k, $k = 0, 1, 2, \ldots, n$, as well as the corresponding values in the ventilated air gap, T_a and e_a.

Knowing the values of these quantities at the previous iteration, the following sequence of actions was performed at the current iteration, and all calculations were performed using the Maple computer algebra system:

1. The equivalent thermal conductivities of the layers containing the closed air gap (Equation (18)) were calculated.
2. For each layer, except for the ventilated air gap, its thermal resistance and vapor permeability resistance were determined according to the expressions $R_k = \delta_k/\lambda_k$ and $R_{vp\,k} = \delta_k/\mu_k$.
3. The value of the heat transfer coefficient on the ventilated air gap walls, $\alpha_{\text{п}}$, was calculated.
4. The reduced heat transfer resistance of the part of the filler structure from the room to the ventilated air gap was determined [36,37,41]:

$$R_{\text{int}} = \frac{1}{\alpha_{\text{int}}} + \sum_{i=1}^{n_{\text{int}}} R_i + \frac{1}{\alpha_a}. \tag{60}$$

5. The value of the heat flow coming from the room to the ventilated air gap was found:

$$q_{\text{int}} = \frac{T_{\text{int}} - T_{\text{п}}}{R_{\text{int}}}. \tag{61}$$

6. Based on (9) and (12), the temperatures at the junction of layers, moving from the room to the ventilated air gap, were found:

$$T_0 = T_{\text{int}} - q_{\text{int}}/\alpha_{\text{int}}, \tag{62}$$

$$T_k = T_{k-1} - q_{\text{int}} \cdot R_k. \tag{63}$$

7. Using (30)–(32), the air velocity in the ventilated air gap v was determined.
8. Using Equations (28) and (29), the air temperatures in the ventilated air gap, $T_{\text{п}}$, and at the exit from it, T_{out}, were calculated.

9. The reduced heat transfer resistance of the filler structure part was calculated from the ventilated air gap to the external filler structure surface (reduced heat transfer resistance of the external facing):

$$R_{\text{ext}} = \frac{1}{\alpha_{\text{ext}}} + \sum_{i=n_{\text{int}}+1}^{n} R_i + \frac{1}{\alpha_a}. \quad (64)$$

10. The value of the heat flow coming from the room to the ventilated air gap was found:

$$q_{\text{ext}} = \frac{T_{\text{ext}} - T_a}{R_{\text{ext}}}. \quad (65)$$

11. Based on (10) and (12), the temperatures at the junction of layers, moving from the external filler structure surface to the ventilated air gap, were found:

$$T_n = T_{\text{ext}} + q_{\text{int}} / \alpha_{\text{ext}}, \quad (66)$$

$$T_{k-1} = T_k + q_{\text{ext}} \cdot R_k. \quad (67)$$

12. The vapor permeability resistance of the filler structure part, from the room to the ventilated air gap, was determined:

$$R_{vp\,\text{int}} = \sum_{i=1}^{n_{\text{int}}} R_{vp\,i}. \quad (68)$$

13. The value of the water vapor flow coming from the room to the ventilated air gap was found:

$$q_{vp\ \text{int}} = \frac{e_{\text{int}} - e_a}{R_{vp\ \text{int}}}. \quad (69)$$

14. Based on (43), the water vapor partial pressure at the junction of layers, moving from the room to the ventilated air gap, was found:

$$e_k = e_{k-1} - q_{vp\ \text{int}} \cdot R_{vp\ k}. \quad (70)$$

15. Using Equations (55) and (56), the water vapor partial pressure in the ventilated air gap, $e_{\text{п}}$, and at the exit from it, e_{out}, was calculated.
16. The vapor permeability resistance of the filler structure part, from the ventilated air gap to the external filler structure surface (vapor permeability resistance of the external facing), was determined [43,44]:

$$R_{vp\,\text{ext}} = \sum_{i=n_{\text{int}}+1}^{n} R_{vp\,i}. \quad (71)$$

17. The value of the water vapor flow coming from the room to the ventilated air gap was found:

$$q_{vp\,\text{ext}} = \frac{e_{vp\,\text{ext}} - e_a}{R_{vp\,\text{ext}}}. \quad (72)$$

18. Based on (43), the partial pressure at the junction of layers, moving from the external filler structure surface to the ventilated air gap, was found:

$$e_{k-1} = e_k + q_{vp\ \text{ext}} \cdot R_{vp\ k}. \quad (73)$$

For the very first iteration, the value of the true thermal conductivity of air can be used as the equivalent coefficient of thermal conductivity in the closed air gap, and in the horizontal air channels λ_e, the water vapor temperature and partial pressure in the ventilated air gap can be determined under the condition of no air flow. Iterations are terminated when the differences between the temperature values at characteristic points in the previous and current iterations become smaller than the pre-set error. The internal and external surfaces of the filler structure and all joints of layers can be used as such characteristic points.

After the completion of the iteration process, the final value of the reduced heat transfer resistance was determined according to (2).

The above method thus allowed us to determine the values of the water vapor temperature and partial pressure on the filler structure surfaces and at the joints of its layers, the density of the heat flow through the filler structure, and its reduced heat transfer resistance. An explanation of the basic values used in the formulas is provided in Appendix A.

After finding these values, if necessary, it is possible to find the distribution of the water vapor temperature and partial pressure throughout the entire filler structure thickness via linear interpolation between the values at the junctions of layers.

The filler structure is checked for the presence of a condensation zone inside it by comparing, at each point along the filler structure thickness, the calculated partial pressure of water vapor and the partial pressure of saturated water vapor at the filler structure temperature established at the corresponding point. At those points where the calculated partial pressure of vapor exceeds the partial pressure of saturated vapor, excess moisture will precipitate in the form of condensate. Note that at such points, the value of the calculated partial pressure has no physical meaning, since in a real situation, as a result of condensation of excess moisture, a partial pressure corresponding to the value of the partial pressure of saturated vapor will be established there. In addition, the purpose of this method is not to determine the actual partial pressure of water vapor in the filler structure. This approach allows us to precisely determine the condensation zones, and it is officially enshrined in regulatory documents [35–38].

3. Results and Discussion

In accordance with the above mathematical models and calculation methods, calculations of the temperature fields and humidity conditions of the filler structures under consideration were performed. In the process of comparative calculations, different values of some geometric parameters were considered, namely, the thickness of the ventilated and the thickness of the closed air gap in Options 2 and 3. Table 2 shows the values of the variable parameters for which the calculations were performed. The last column of this table shows the designations that are used below for a brief designation of the filler structure under consideration.

Table 3 shows the calculated reduced heat transfer resistance and heat flow density passing from the room to the outside for each considered option, as well as some thermophysical parameters of the ventilated air gap: average air temperature and air temperature at the exit of the gap, and the reduced (considering the radiant component) heat transfer coefficient on the ventilated air gap wall. The data in Table 4 reflect the quite obvious fact that the application of a heat-reflecting coating led to an improvement in the heat-protective properties of the filler structure produced according to the same scheme and with the same geometric parameters, but without a heat-reflecting coating.

Table 4. Main thermophysical parameters of the considered options for filler structures.

Filler Structure Option	Reduced Heat Transfer Resistance R, (°C·m^2)/W	Heat Flow Density Passing Through the Filler Structure, q, W/m^2	Air Velocity in the Ventilated Air Gap v, m/s	Average Air Temperature in the Ventilated Air Gap T_{in}, °C	Air Temperature at the Exit of the Ventilated Air Gap T_{out}, °C	Heat Transfer Coefficient on the Air Gap Wall α_{in}, W/(m^2·K)
Option 1	3.612	9.773	0.317	−13.66	−13.02	11.99
Option 2/175/25	3.832	9.211	0.319	−13.65	−13.00	12.00
Option 2/150/50	3.836	9.201	0.329	−13.61	−12.92	12.03
Option 2/125/75	3.842	9.189	0.340	−13.56	−12.82	12.07
Option 2/100/100	3.848	9.174	0.354	−13.50	−12.70	12.12
Option 2/75/125	3.855	9.156	0.369	−13.43	−12.56	12.17
Option 2/50/150	3.864	9.135	0.386	−13.35	−12.39	12.24
Option 2/25/175	3.874	9.111	0.405	−13.25	−12.20	12.31
Option 3/175/25	4.270	8.271	0.306	−13.70	−13.11	11.95
Option 3/150/50	4.273	8.262	0.315	−13.67	−13.03	11.98
Option 3/125/75	4.278	8.252	0.326	−13.62	−12.94	12.02
Option 3/100/100	4.285	8.237	0.338	−13.57	−12.84	12.07
Option 3/75/125	4.293	8.222	0.353	−13.51	−12.71	12.12
Option 3/50/150	4.302	8.205	0.368	−13.43	−12.56	12.17
Option 3/25/175	4.313	8.185	0.386	−13.35	−12.40	12.23

To conduct a comparative analysis of the thermal protection properties of the filler structures of various design schemes and with various geometric parameters, we calculated the relative (in percent) change in the value of the reduced heat transfer resistance in relation to a traditional filler structure (Option 1). In this case, we separately compared filler structures with a heat-reflecting coating and filler structures without a heat-reflecting coating. The corresponding data are provided in Table 5.

Table 5. Absolute and relative values of the reduced heat transfer resistance.

Filler Structure Option	Reduced Heat Transfer Resistance, (°C·m^2)/W		Increase in the Reduced Heat Transfer Resistance Compared to Traditional Filler Structure, %		Increase in the Reduced Heat Transfer Resistance Due to Application of Heat-Reflecting Coating, %
	Without Heat-Reflecting Coating	With Heat-Reflecting Coating	Without Heat-Reflecting Coating	With Heat-Reflecting Coating	
Option 1	3.612	3.708	-	-	2.66
Option 2, 3/175/25	3.832	4.270	6.09	15.16	11.43
Option 2, 3/150/50	3.836	4.273	6.20	15.24	11.39
Option 2, 3/125/75	3.842	4.278	6.37	15.37	11.35
Option 2, 3/100/100	3.848	4.285	6.53	15.56	11.36
Option 2, 3/75/125	3.855	4.293	6.73	15.78	11.36
Option 2, 3/50/150	3.864	4.302	6.98	16.02	11.34
Option 2, 3/25/175	3.874	4.313	7.25	16.32	11.33

As can be seen from Table 5, the filler structure produced according to Option 2 allowed us to increase the value of the reduced heat transfer resistance by 6.1–7.2%, in comparison with the traditional filler structure produced according to Option 1 (in the absence of a heat-reflecting coating), and by 15.2–16.3% compared to that produced according to Option 3 (in the presence of a heat-reflecting coating). In this case, a clear dependence was observed: with an increase in the thickness of the closed air gap (with the sum of the thicknesses of the closed and ventilated air gaps remaining unchanged), the value of the reduced heat transfer resistance of the filler structure produced according to Option 2 increased slightly, from 3.832 to 3.874 (°C·m^2)/W in the filler structures without a heat-reflecting coating, and from 4.270 to 4.313 (°C·m^2)/W in the filler structures with a heat-reflecting coating

(Option 3). In relative terms, these increases were 1.1% and 1.0%, respectively. In the last column of Table 4, the data also show that the application of a heat-reflecting coating to the filler structure produced according to Option 3, regardless of the selected values of the variable geometric parameters, led to an improvement in its heat-protective properties by approximately 11.3–11.4%, which is significantly more than in the case of Option 1 (2.66%) [42].

Table 6 shows the temperature values on the internal (T_0) and external (T_n) surfaces of the filler structure, as well as at the joints of layers (T_1, T_2, …, T_7). Based on these data, the temperature distribution graphs below were constructed. According to the methodology described in the previous section, these graphs were constructed as a result of linear interpolation between Table 6 data.

Table 6. Temperatures on the internal and external surfaces of the filler structures and at the junction of layers, °C.

Filler Structure Option	T_0	T_1	T_2	T_3	T_4	T_5	T_6	T_7	T_n
Option 1	19.88	19.75	13.35	13.22	−12.84	−14.13	-	-	−14.14
Option 2/175/25	19.94	19.82	13.79	13.66	−1.69	−3.67	−12.88	−14.13	−14.14
Option 2/150/50	19.94	19.82	13.79	13.67	−1.66	−3.64	−12.84	−14.11	−14.12
Option 2/125/75	19.94	19.82	13.80	13.68	−1.63	−3.61	−12.80	−14.09	−14.11
Option 2/100/100	19.95	19.82	13.81	13.69	−1.60	−3.57	−12.74	−14.07	−14.09
Option 2/75/125	19.95	19.83	13.83	13.71	−1.55	−3.52	−12.68	−14.04	−14.06
Option 2/50/150	19.95	19.83	13.84	13.72	−1.50	−3.46	−12.60	−14.01	−14.02
Option 2/25/175	19.95	19.83	13.86	13.74	−1.44	−3.40	−12.51	−13.95	−13.97
Option 3/175/25	20.05	19.94	14.52	14.41	0.63	−4.74	−13.01	−14.14	−14.15
Option 3/150/50	20.05	19.94	14.53	14.42	0.65	−4.71	−12.98	−14.13	−14.14
Option 3/125/75	20.05	19.94	14.54	14.43	0.68	−4.68	−12.93	−14.11	−14.12
Option 3/100/100	20.05	19.94	14.55	14.44	0.71	−4.65	−12.89	−14.09	−14.10
Option 3/75/125	20.05	19.95	14.56	14.45	0.75	−4.61	−12.83	−14.07	−14.08
Option 3/50/150	20.06	19.95	14.57	14.47	0.79	−4.55	−12.76	−14.03	−14.05
Option 3/25/175	20.06	19.95	14.59	14.48	0.84	−4.50	−12.68	−13.98	−14.00

As can be seen from Table 5, the temperature of the internal filler structure surface for all the options was considered in the range of 19.2–20.1 °C. The temperature difference between the temperature of the internal air (21 °C) and the temperature of the internal filler structure surface (T_0) for all the options considered was thus in the range of 0.9–1.8 °C. These values did not exceed the standard value of this parameter (4.0 °C for the external walls of residential buildings, medical and preventive care facilities, and children's institutions), as given in [34,35].

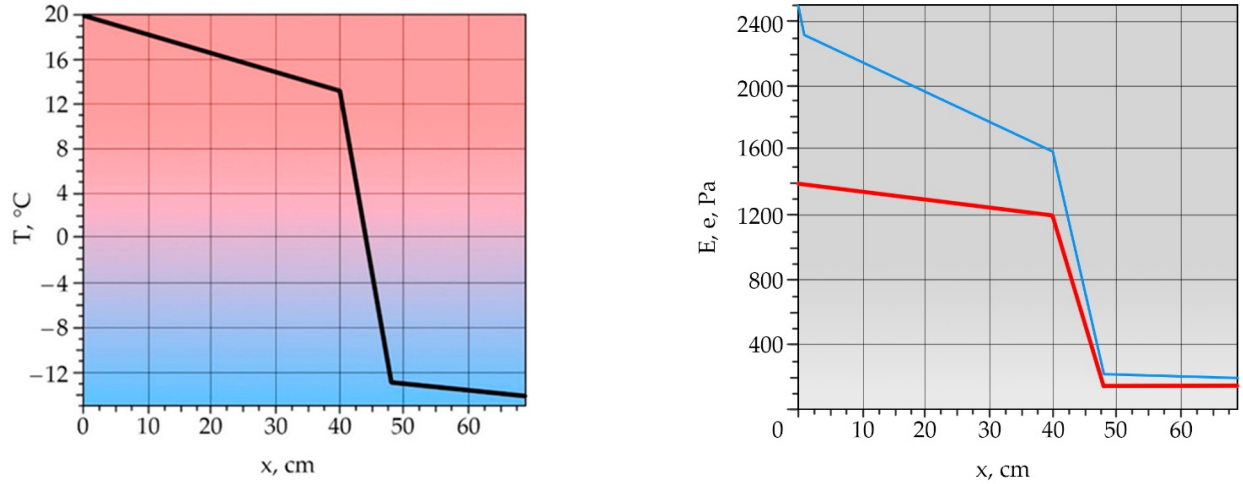
Negative temperatures in the filler structure made according to Option 1 were observed in the thermal insulation layer made of extruded cellular polystyrene and further to the external filler structure surface. In all versions of the filler structures made according to Options 2 and 3, negative temperatures were observed starting from the closed air gap and further to the external filler structure surface.

In Table 7, for each option of the filler structure, the first row shows the calculated values of the water vapor partial pressure on the internal and external surfaces of the filler structure and at the junction of layers. The second row for each option of the filler structure shows the values of the saturated water vapor partial pressure determined using the calculated temperatures at the corresponding points, i.e., using the temperatures from Table 6. The penultimate column for each option of the filler structure shows the minimum (among all junctions of layers) difference between the saturated vapor partial pressure and the calculated partial pressure. The last column shows the numbers of layers at the junction at which this maximum difference was observed. A negative value of this maximum difference indicates that the calculated partial pressure of water vapor exceeded the partial pressure of saturated vapor. In this case, excess moisture precipitates in the corresponding part of the filler structure in the form of condensate [42].

Table 7. Partial pressure of water vapor on the internal and external surfaces of the filler structures and at the junction of layers, Pa.

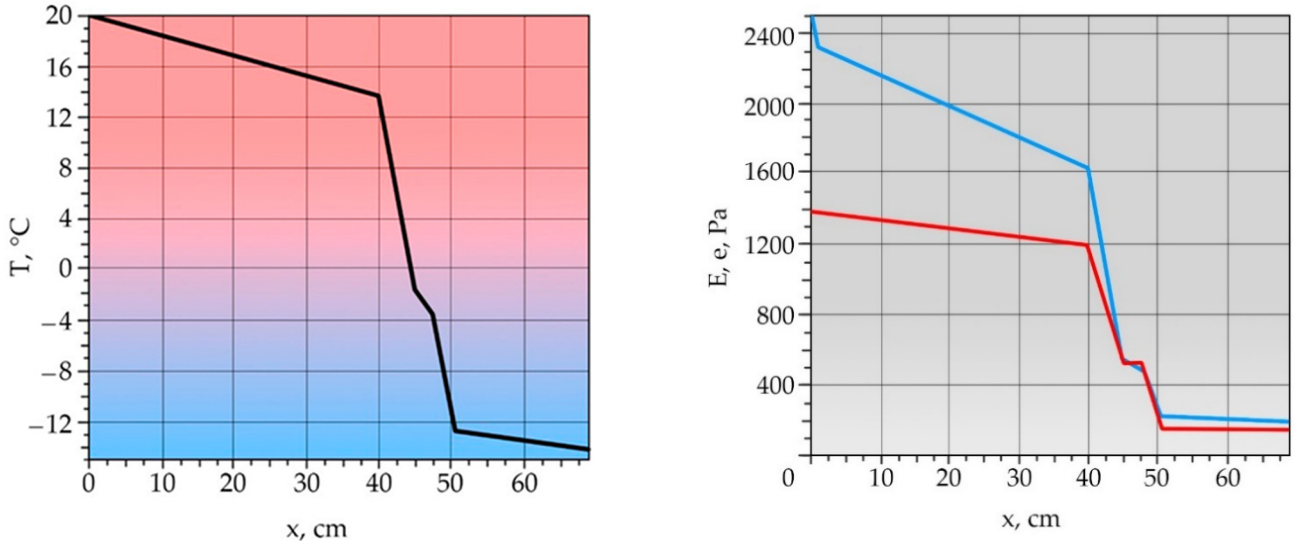
Filler Structure Option	e_0	e_1	e_2	e_3	e_4	e_5	e_6	e_7	e_n	$(E-e)_{max}$	Layer Numbers
Option 1	1391 2529	1384 2310	1204 1599	1197 1585	141 215	141 195	- -	- -	141 192	52	6
Option 2/175/25	1391 2529	1384 2318	1204 1648	1197 1635	537 552	537 482	141 215	141 195	141 192	−55	5–6
Option 2/150/50	1391 2529	1384 2318	1204 1649	1197 1636	537 553	537 483	141 215	141 195	141 192	−54	5–6
Option 2/125/75	1391 2529	1384 2318	1204 1650	1197 1637	537 554	537 484	141 216	141 196	141 192	−53	5–6
Option 2/100/100	1391 2529	1384 2319	1204 1651	1197 1638	537 555	537 486	141 217	141 196	141 192	−51	5–6
Option 2/75/125	1391 2529	1384 2319	1204 1653	1197 1640	537 556	537 487	141 218	141 197	141 192	−50	5–6
Option 2/50/150	1391 2529	1384 2319	1204 1655	1197 1641	537 558	537 489	142 219	142 197	141 192	−48	5–6
Option 2/25/175	1391 2529	1384 2319	1205 1657	1197 1644	538 560	538 492	143 221	143 198	141 192	−46	5–6
Option 3/175/25	1391 2529	1384 2331	1204 1730	1197 1718	537 650	537 445	141 213	141 195	141 192	−92	5–6
Option 3/150/50	1391 2529	1384 2332	1204 1731	1197 1719	537 651	537 446	141 213	141 195	141 192	−91	5–6
Option 3/125/75	1391 2529	1384 2332	1204 1732	1197 1720	537 653	537 447	141 214	141 195	141 192	−90	5–6
Option 3/100/100	1391 2529	1384 2332	1204 1733	1197 1721	537 655	537 448	141 215	141 196	141 192	−89	5–6
Option 3/75/125	1391 2529	1384 2332	1204 1734	1197 1722	537 657	537 449	141 216	141 196	141 192	−88	5–6
Option 3/50/150	1391 2529	1384 2332	1204 1736	1197 1724	537 660	537 451	142 217	142 197	141 192	−86	5–6
Option 3/25/175	1391 2529	1384 2333	1205 1737	1197 1725	538 663	538 453	143 218	143 197	141 192	−85	5–6

As can be seen from Table 7, the presence of condensation zones was observed in all filler structures produced according to Options 2 and 3, regardless of whether they had a heat-reflecting screen or not. However, according to the value of the inadmissibility of moisture accumulation in multilayer structures of external enclosures, over the annual period of operation, the structures complied with the requirements of [36]. Graphic dependencies of the changes in temperature and partial pressure of water vapor across the filler structure thickness are shown in Figures 2–16. In this case, the red line corresponds to the calculated values of the water vapor partial pressure, and the blue line represents the values of the saturated water vapor partial pressure for the calculated temperature at each point of the filler structure. The criterion for non-condensation in the filler structure is that the calculated partial pressure should be less than the partial pressure of saturated water vapor. The intersection of the red and blue lines on the pressure graph thus indicates that this filler structure is unsuitable for use in the climatic conditions under consideration due to the presence of condensation zones in it. These graphs also make it easy to visually determine the condensation zone: it is located where the red line is above the blue line on the graph. An analysis of the pressure graphs and values given in Table 6 allowed us to draw the following conclusions about the location of condensation zones. In all the considered options of the filler structures made according to Options 2 and 3, the condensation zone was located in the closed air gap and in the external layer of thermal insulation produced with extruded cellular polystyrene.



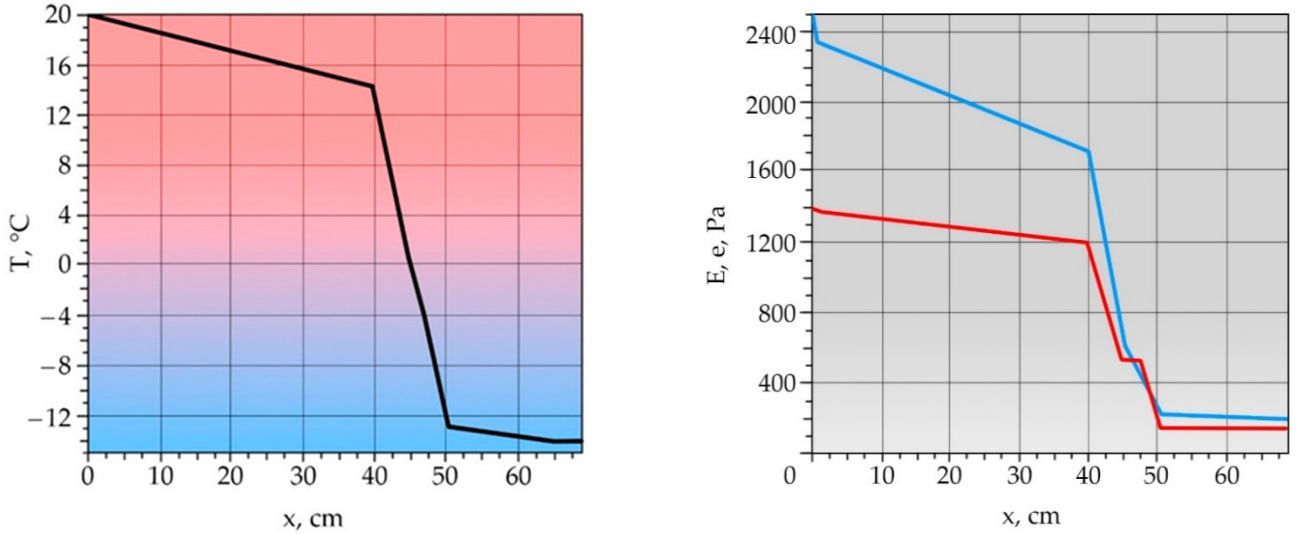
(**a**) (**b**)

Figure 2. Changes in temperature and humidity parameters across the filler structure thickness for Option 1: (**a**) temperature and (**b**) partial pressure of water vapor (red line: calculated value; blue line: partial pressure of saturated water vapor).



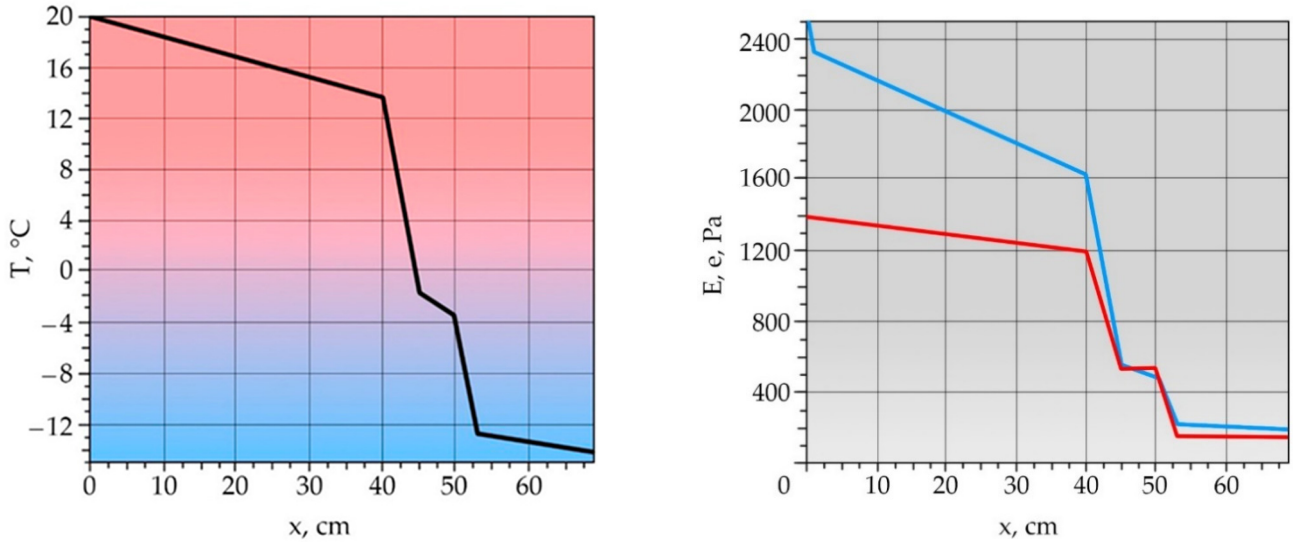
(**a**) (**b**)

Figure 3. Changes in temperature and humidity parameters across the filler structure thickness for Option 2/175/25: (**a**) temperature and (**b**) partial pressure of water vapor (red line: calculated value; blue line: partial pressure of saturated water vapor).



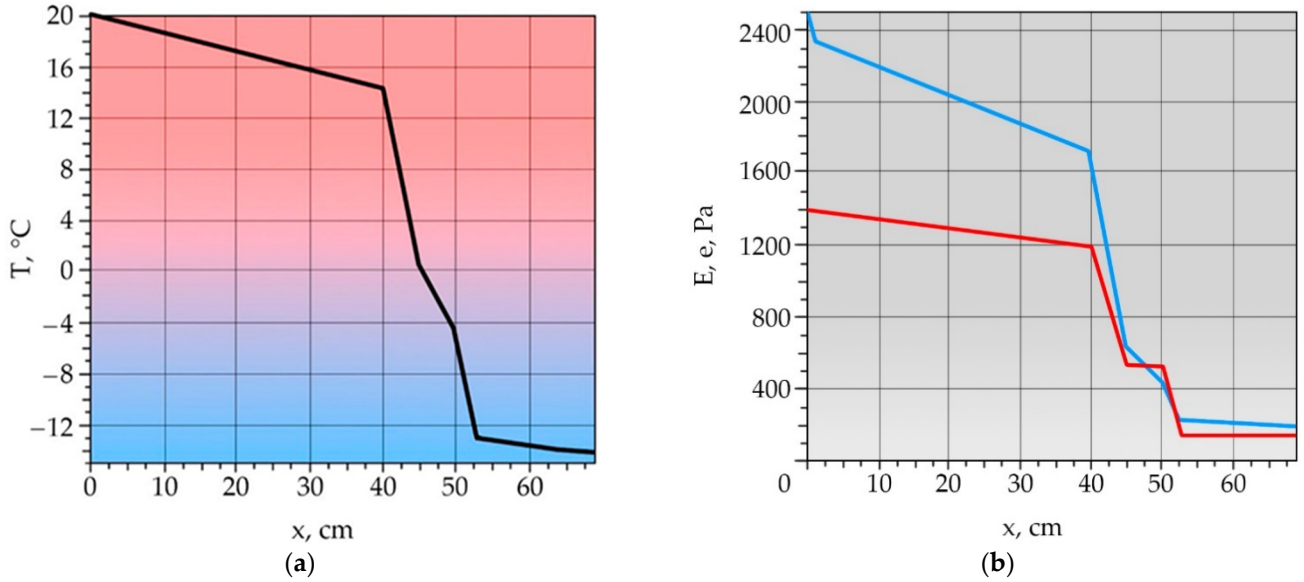
(**a**) (**b**)

Figure 4. Changes in temperature and humidity parameters across the filler structure thickness for Option 3/175/25: (**a**) temperature and (**b**) partial pressure of water vapor (red line: calculated value; blue line: partial pressure of saturated water vapor).



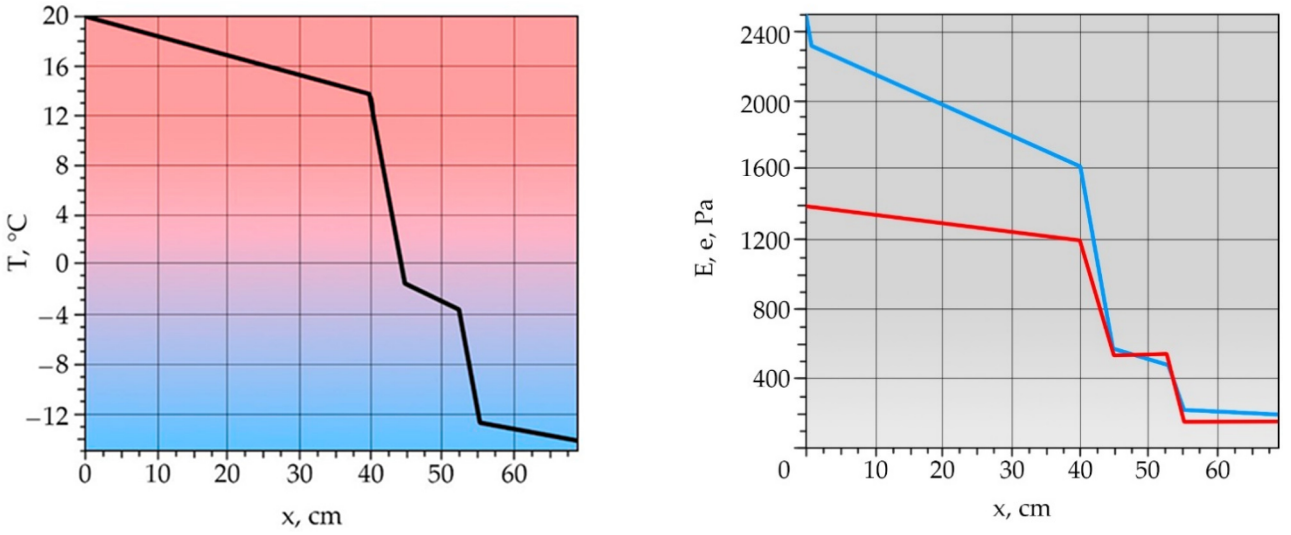
(**a**) (**b**)

Figure 5. Changes in temperature and humidity parameters across the filler structure thickness for Option 2/150/50: (**a**) temperature and (**b**) partial pressure of water vapor (red line: calculated value; blue line: partial pressure of saturated water vapor).



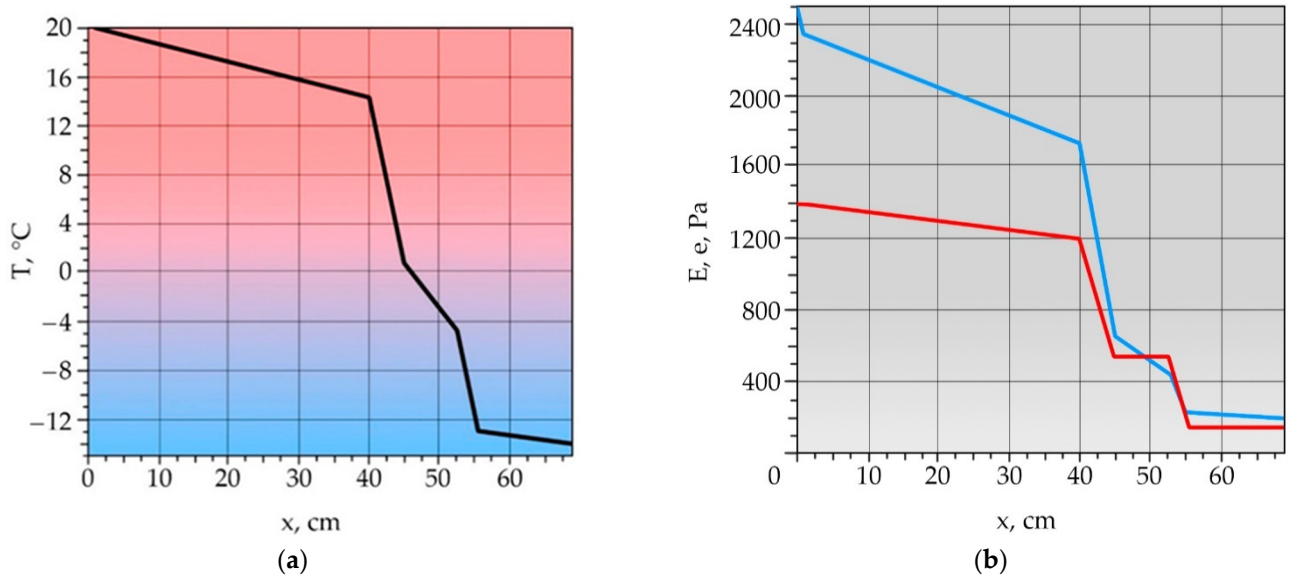
(**a**) (**b**)

Figure 6. Changes in temperature and humidity parameters across the filler structure thickness for Option 3/150/50: (**a**) temperature and (**b**) partial pressure of water vapor (red line: calculated value; blue line: partial pressure of saturated water vapor).



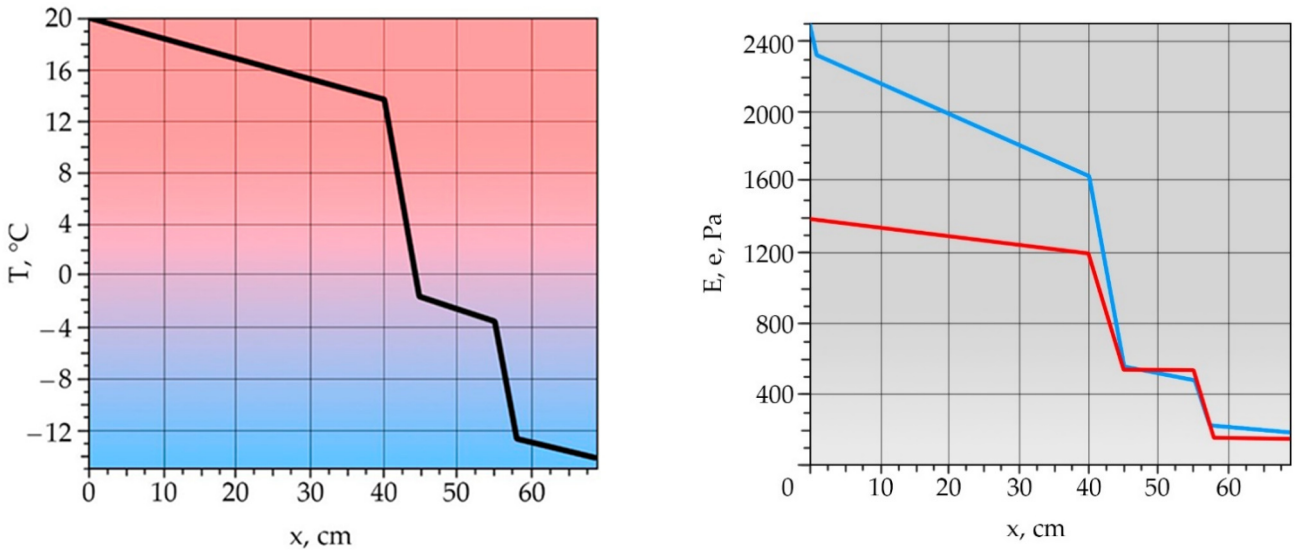
(**a**) (**b**)

Figure 7. Changes in temperature and humidity parameters across the filler structure thickness for Option 2/125/75: (**a**) temperature and (**b**) partial pressure of water vapor (red line: calculated value; blue line: partial pressure of saturated water vapor).



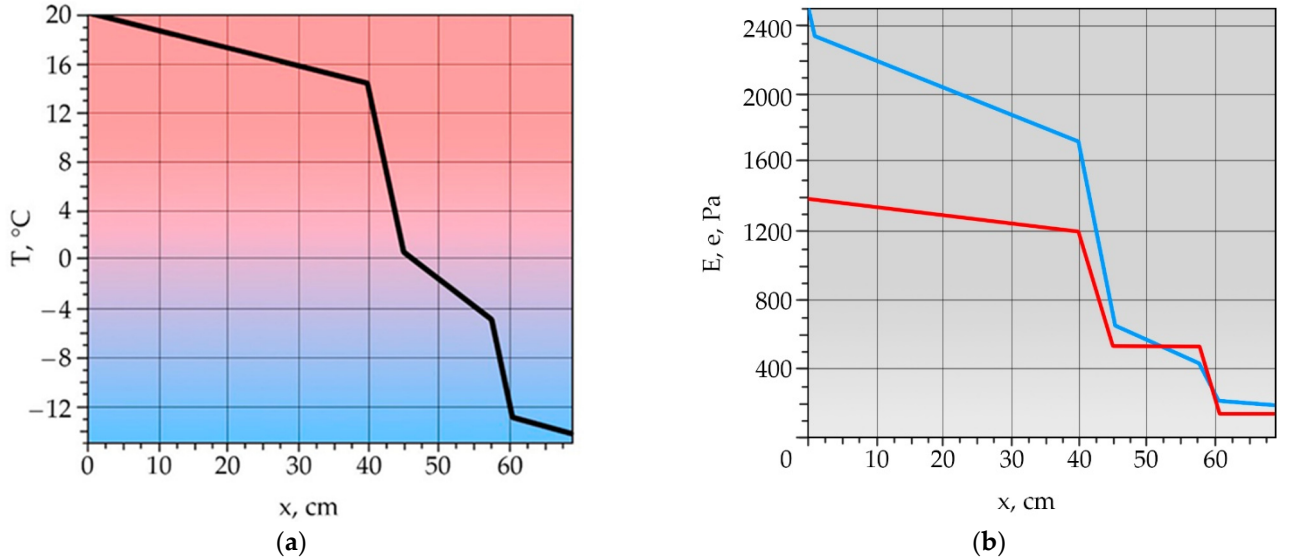
(**a**) (**b**)

Figure 8. Changes in temperature and humidity parameters across the filler structure thickness for Option 3/125/75: (**a**) temperature and (**b**) partial pressure of water vapor (red line: calculated value; blue line: partial pressure of saturated water vapor).



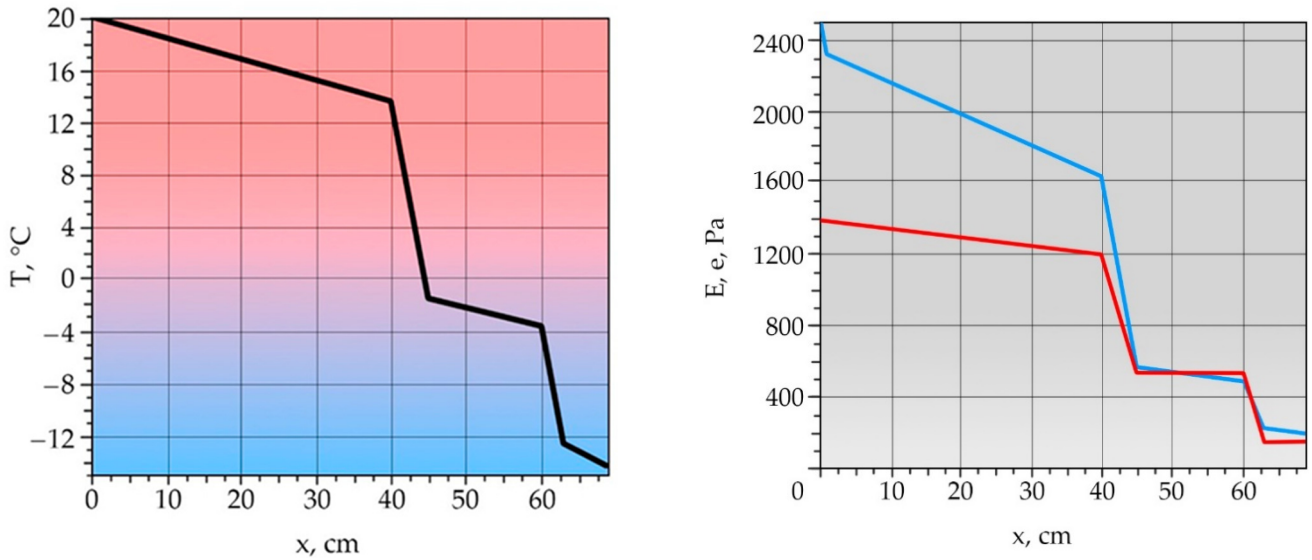
(**a**) (**b**)

Figure 9. Changes in temperature and humidity parameters across the filler structure thickness for Option 2/100/100: (**a**) temperature and (**b**) partial pressure of water vapor (red line: calculated value; blue line: partial pressure of saturated water vapor).



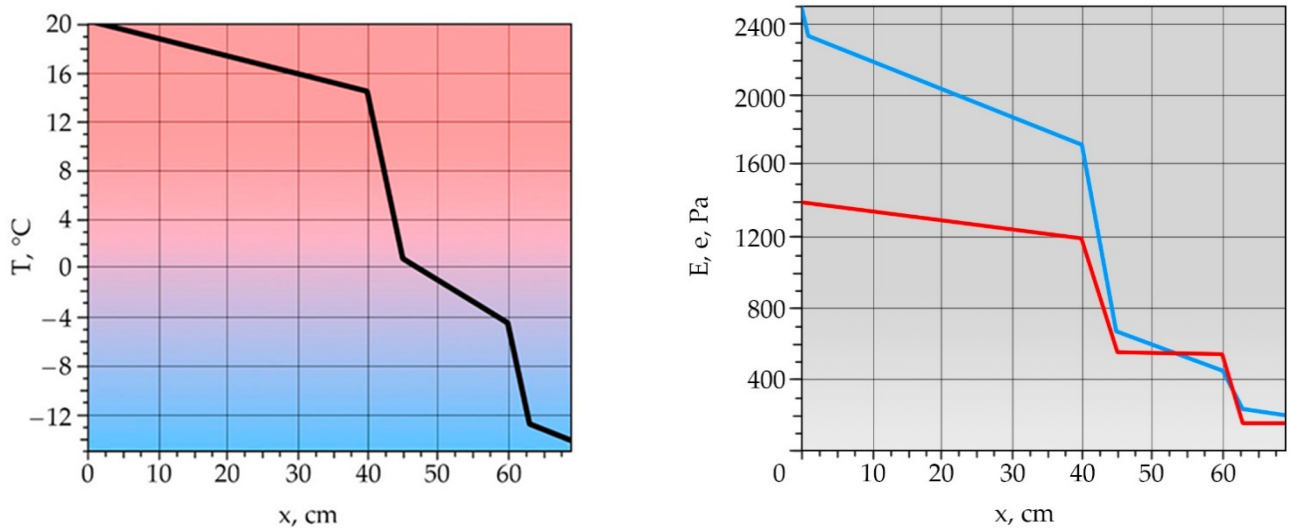
(**a**) (**b**)

Figure 10. Changes in temperature and humidity parameters across the filler structure thickness for Option 3/100/100: (**a**) temperature and (**b**) partial pressure of water vapor (red line: calculated value; blue line: partial pressure of saturated water vapor).



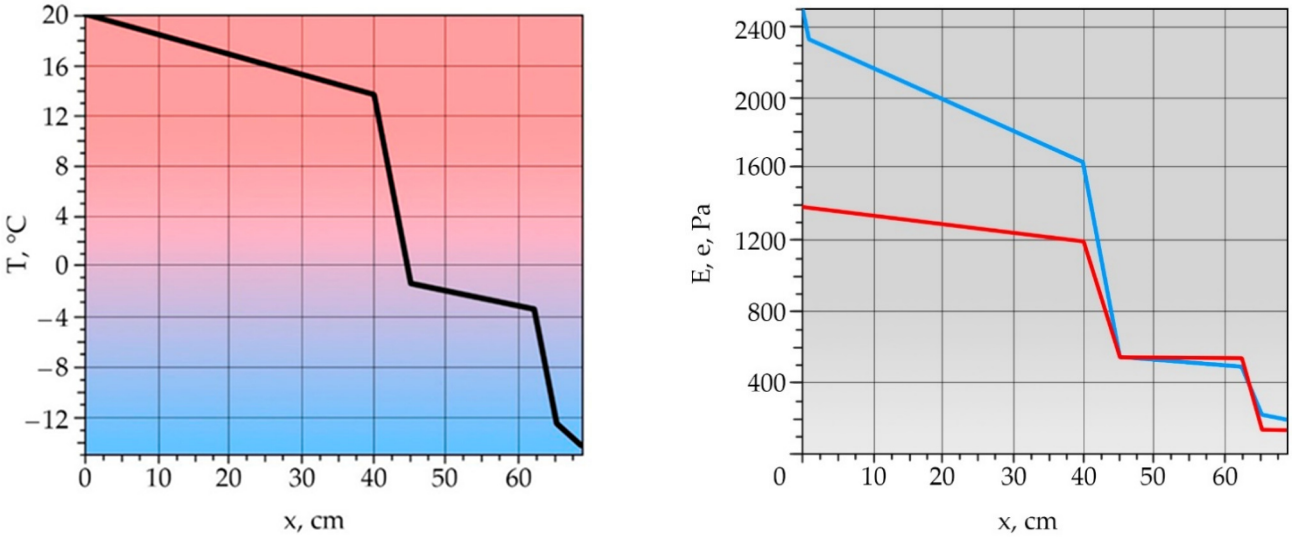
(**a**) (**b**)

Figure 11. Changes in temperature and humidity parameters across the filler structure thickness for Option 2/75/125: (**a**) temperature and (**b**) partial pressure of water vapor (red line: calculated value; blue line: partial pressure of saturated water vapor).



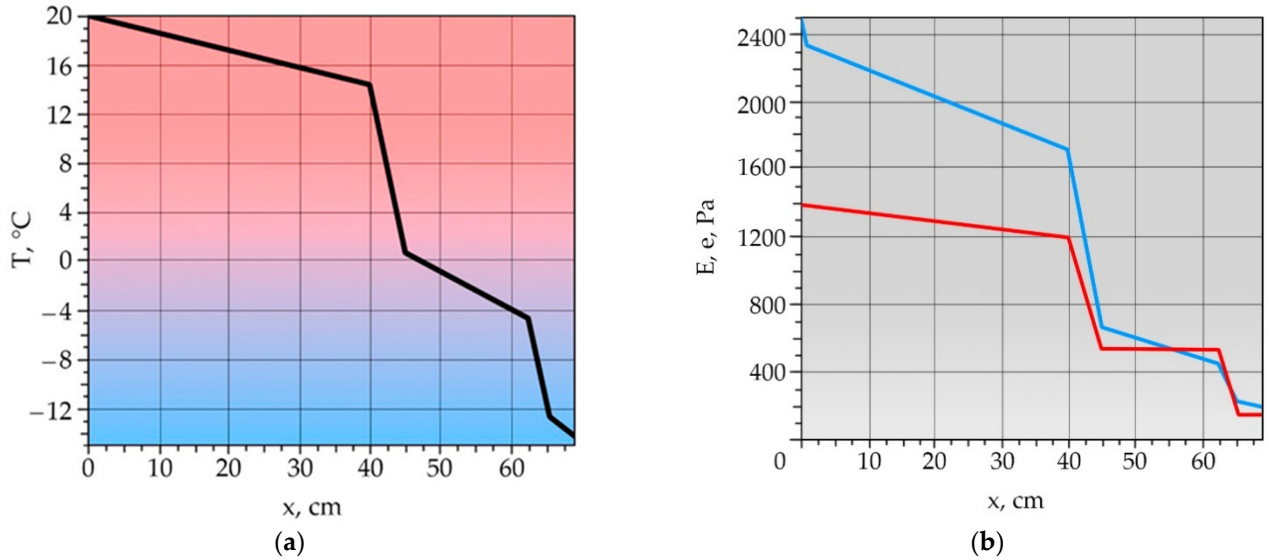
(**a**) (**b**)

Figure 12. Changes in temperature and humidity parameters across the filler structure thickness for Option 3/75/125: (**a**) temperature and (**b**) partial pressure of water vapor (red line: calculated value; blue line: partial pressure of saturated water vapor).



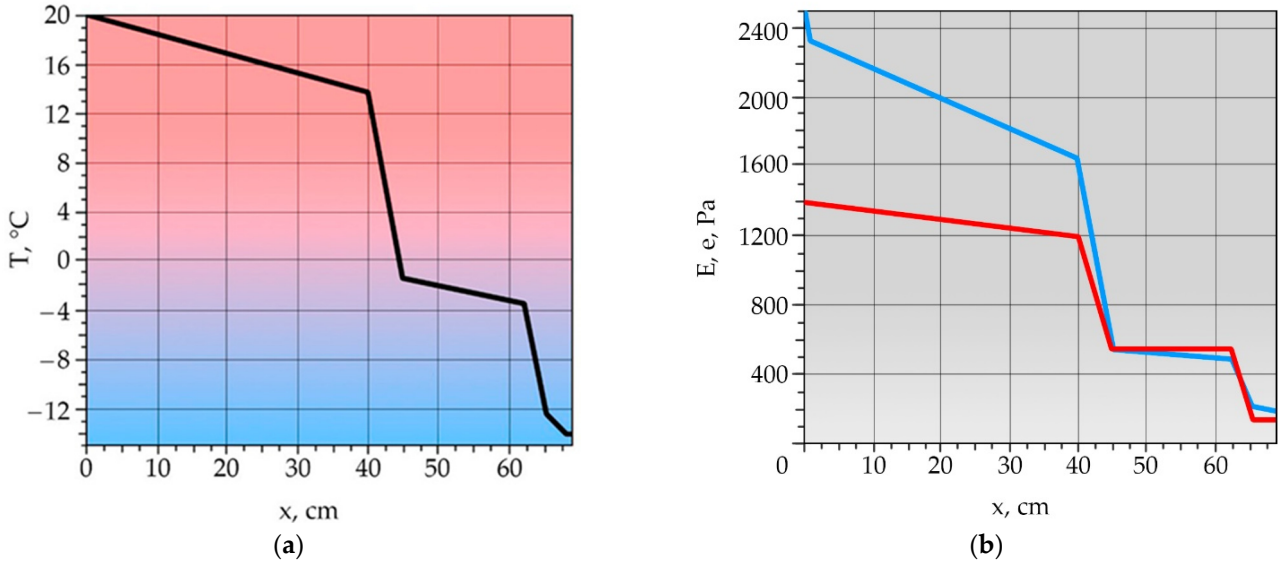
(**a**) (**b**)

Figure 13. Changes in temperature and humidity parameters across the filler structure thickness for Option 2/50/150: (**a**) temperature and (**b**) partial pressure of water vapor (red line: calculated value; blue line: partial pressure of saturated water vapor).



(**a**) (**b**)

Figure 14. Changes in temperature and humidity parameters across the filler structure thickness for Option 3/50/150: (**a**) temperature and (**b**) partial pressure of water vapor (red line: calculated value; blue line: partial pressure of saturated water vapor).



(**a**) (**b**)

Figure 15. Changes in temperature and humidity parameters across the filler structure thickness for Option 2/25/175: (**a**) temperature and (**b**) partial pressure of water vapor (red line: calculated value; blue line: partial pressure of saturated water vapor).

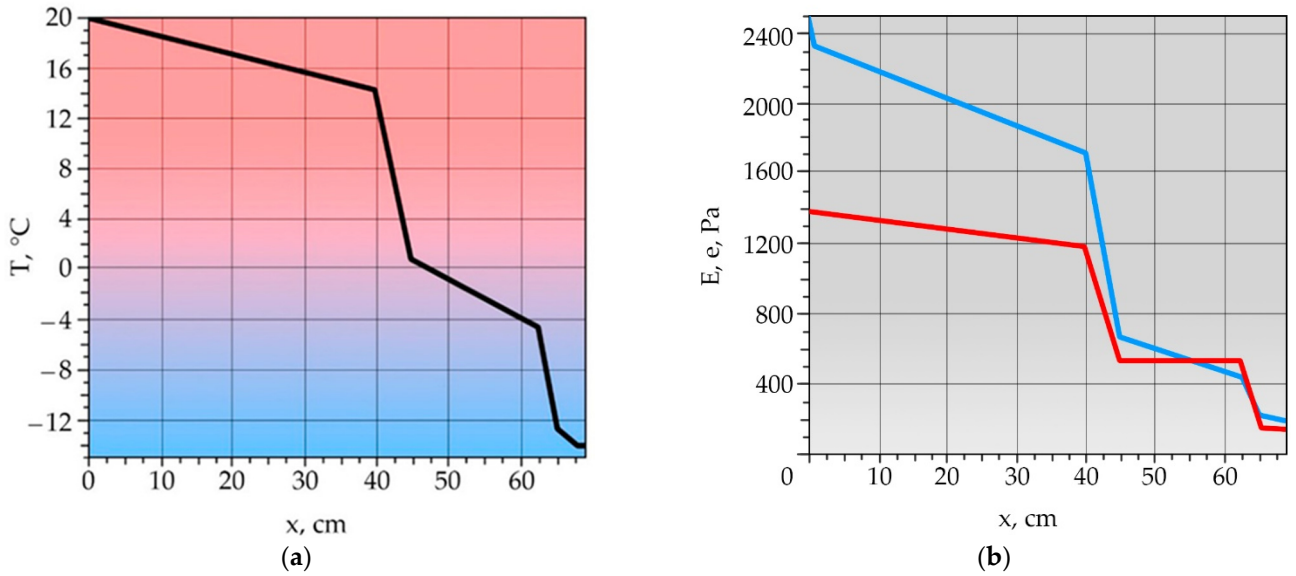


Figure 16. Changes in temperature and humidity parameters across the filler structure thickness for Option 3/25/175: (**a**) temperature and (**b**) partial pressure of water vapor (red line: calculated value; blue line: partial pressure of saturated water vapor).

The primary aim of developing this topic was to investigate the climatic features of the study region. Since the region belongs to the III and IV [34] climatic regions, this design will be relevant for the availability of construction solutions, such as using a closed air gap, ventilated air gap, and heat-reflecting screens to optimize the thermal characteristics of structures in winter. However, the III and IV [34] climatic regions are characterized by hot summers in addition to cold winters, which is also relevant. The purpose of the developed design is that in winter, a closed layer acts as thermal insulation, and in summer, it will serve as an additional ventilated layer [11], which will significantly affect energy savings, and the results of this analysis will be presented in subsequent research. In addition, the authors, having researched and developed a new energy-saving design for detailed analysis, have developed new mathematical models of heat transfer and water vapor filtration through wall fences, while also considering design features. As a result, a variable analysis of different geometric parameters was carried out, and the most effective design was determined.

4. Conclusions

First, we developed a new energy-efficient multilayer enclosing structure and developed new mathematical models of heat transfer and water vapor filtration for analysis, considering different geometric parameters of the structure in the cold climate of the study region. We then conducted a timely comparison of the newly developed design with the traditional one for the effectiveness of using one or another construction device. The results showed that the reduced heat transfer resistance of a traditional enclosing structure, which has a layer of solid insulation and a ventilated air layer, was 6.1–7.2% lower than the reduced heat transfer resistance of a developed facade with closed and ventilated air layers. In the case of a heat-reflecting coating, the difference between these values increased to 15.2–16.3%. However, considering all the filler structure geometry options with closed and ventilated air gaps, there were still water vapor condensation zones, but according to the value of the inadmissibility of moisture accumulation in multilayer structures of wall structures, over the annual period of operation, the structures complied with the standard climatic conditions of Shymkent (the average temperature of the coldest five-day period was −14.3 °C). However, it should be noted that in warmer climates, the temperature

inside the filler structure will rise above the dew point, and water vapor condensation will not occur. Negative temperatures in the considered filler structures were observed starting from the closed air gap or continuous layer of thermal insulation made of extruded cellular polystyrene and further to the external surface. The bearing layers were thus not subject to freezing during operation for all considered filler structures. As a limitation of this study, it can be noted that we did not conduct calculations considering heterogeneous inclusions (cold bridges); however, this limitation does not reduce the significance of the theoretical studies and will be further investigated in our upcoming works.

To summarize the above, it can be concluded that the developed energy-efficient wall structure is suitable for the climatic conditions of Shymkent, since it exhibited better thermal insulation properties than the traditional ventilated facade with a continuous layer of thermal insulation. In addition, the use of a heat-reflecting coating led to a 16.3% improvement in the thermal protection properties of the developed facade (depending on its geometric parameters) compared to a similar filler structure that does not have a heat-reflecting coating, which was patented [45].

Author Contributions: Conceptualization, N.Z. and T.T.; methodology, N.Z. and A.U.; investigation, N.Z. and U.A.; data curation, T.T. and A.U.; writing—original draft preparation, N.Z. and U.A.; writing—review and editing, N.Z. and M.S.; supervision, N.Z.; project administration, N.Z.; funding acquisition, N.Z. and M.S. All authors have read and agreed to the published version of the manuscript.

Funding: This research received no external funding.

Data Availability Statement: Data are contained within the article.

Acknowledgments: As a result of this research conducted on the development of energy-efficient wall fencing, a patent for the invention was published in the Republic of Kazakhstan [45]: Multilayer energy-saving wall enclosing structure with air layers, 2024, No. 36864.

Conflicts of Interest: The authors declare that they have no known competing financial interests or personal relationships that could have appeared to influence the work reported in this article.

Appendix A

R	the heat transfer resistance of a multilayer filler structure, °C·m^2/W
α_{int}	the heat transfer coefficient on the internal filler structure surface, W/(m^2·°C)
δ_i	the thickness of the i-th layer, m
λ_i	the thermal conductivity coefficient of the i-th layer material, W/(m·°C)
α_{ext}	the heat transfer coefficient on the external filler structure surface
T_{int}	the estimated inside air temperature, °C
T_{ext}	the estimated outside air temperature, °C
A	the surface area of the considered enclosing covering fragment, m^2
Q	the total heat flow passing through the considered structure fragment, W
x_0	the coordinate of the internal filler structure surface
x_k	the coordinate of the junction of layers with numbers x_k and x_{k+1} ($k = 1, \ldots, n-1$)
n	the number of layers in the filler structure
x_n	the coordinate of the external filler structure surface
λ_k	the thermal conductivity coefficient, W/(m·°C)
$T = T(x)$	the spatial change in the filler structure temperature, °C
q_k	the density of the conductive–convective heat flow component, W/m^2
q_r	the density of the radiant heat flow component, W/m^2
λ_t	the true value of the thermal conductivity coefficient of air, W/(m·°C)

Ra	the Rayleigh number
g	the acceleration due to gravity, m^2/s^2
δ	the air gap thickness, which in our case is equal to the layer δ_k thickness, m
β	the coefficient of volumetric thermal expansion, which for air under normal conditions can be taken as equal to 1/273 °C
ΔT	the temperature difference on the opposite air gap walls (in our case $\Delta T = T_{k-1} - T_k$), °C
ν	the coefficient of kinematic viscosity of air at average values of temperature and pressure in the air gap
Pr	the Prandtl number
σ_0	the Stefan–Boltzmann constant, $5.67 \cdot 10^{-8}$ W/(m^2·K^4)
ε	the reduced emissivity factor, which, in the case of two flat parallel walls of great length, can be calculated according to the expression $\frac{1}{\varepsilon} = \frac{1}{\varepsilon_{k-1}} + \frac{1}{\varepsilon_k} - 1$
ε_{k-1} and ε_k	the emissivity factor of the walls (in our case, the solid surfaces at the corresponding joints of the filler structure layers)
$T = T(\tau, x, y, z)$	the temperature field in the air moving in the gap, °C
c	the heat capacity of the air, J/K
ρ	the air density, kg/m^3
q_V	the specific volumetric density of internal heat sources, W/m^2
λ	the thermal conductivity of the air, W/(m·°C)
v	the air velocity in the ventilated gap, m/s
z	the vertical coordinate
α_a	the heat transfer coefficient on the gap walls, assumed to be the same on the internal and external walls due to the assumption that the air velocity at each point of the gap is the same, W/(m·°C)
T_{k-1}	the temperature on the internal wall limiting the gap, °C
T_k	the temperature on the external wall limiting the gap, °C
H	the difference in height between the supply and exhaust openings of the ventilated air gap, m
Δp^o	the total losses of total pressure, Pa
p_c	the driving pressure (stack effect), Pa
ξ	the sum of local hydraulic resistances
ρ_a	the average air density in the gap (air density at temperature $T_п$), kg/m^3
ρ_{ext}	the atmospheric air density (air density at temperature T_{ext}), kg/m^3
ρ_{out}	the air density at the exit from the gap (air density at temperature T_{out}), kg/m^3
q_{vp}	the value of the water vapor flow passing through the filler structure from the room to the outside, g/m^2/t
μ	the vapor permeability coefficient, mg/(m·h·Pa)
e	the partial pressure of water vapor in the air, Pa
e_{k-1}, e_k	the partial pressure of water vapor on the opposite surfaces of the layer under consideration, Pa
μ_i	the vapor permeability coefficient of the material from which the i-th layer is produced, mg/(m·h·Pa)
n_{int}	the number of layers under consideration from the room to the ventilated air gap
$q_{vp\ int}$ and $q_{vp\ ext}$	the values of the water vapor flow from the room to the ventilated air gap and through the external facing, respectively
$m(z)$	the mass of the water vapor in the corresponding horizontal section of the ventilated air gap, g/m^3
$\rho(z)$	the density of the water vapor in the corresponding horizontal section of the ventilated air gap, kg/m^3
$d\tau$	the time interval during which the air, rising in the ventilated air gap, passes the distance dz, in seconds

References

1. Energimyndigheten. Available online: https://www.energimyndigheten.se/forskning-och-innovation/ (accessed on 17 December 2024).
2. Shandilya, A.; Streicher, W. Performance and Cost Analysis of Retrofit Strategies Applied to a Sample Single Family House Located in New Delhi India Assisted by TRNSYS Energy Simulation Tool-A Case Study. *Int. J. Eng. Tech. Res.* **2017**, *6*, 304–312. [CrossRef]
3. Shandilya, A.; Hauer, M.; Streicher, W. Optimization of Thermal Behavior and Energy Efficiency of a Residential House Using Energy Retrofitting in Different Climates. *Civ. Eng. Archit.* **2020**, *8*, 335–349. [CrossRef]
4. IEA. *Energy Efficiency 2020*; IEA: Paris, France, 2020. Available online: https://www.iea.org/reports/energy-efficiency-2020 (accessed on 17 December 2024).
5. Dubrakova, O.K. Optimization of thermal modernization of a group of buildings using simulation modeling. *J. Appl. Eng. Sci.* **2019**, *17*, 192–197. [CrossRef]

6. Alsabry, A.; Truszkiewicz, P.; Szymański, K.; Łaskawiec, K.; Rojek, Ł. Analysis of energy consumption and possibilities of thermal-modernization in residential buildings in Poland case study: The town of Zielona Góra. *Int. J. Appl. Mech. Eng.* **2017**, *22*, 1083–1095. [CrossRef]
7. Zhangabay, N.; Abshenov, K.; Bakhbergen, S.; Zhakash, A.; Moldagaliyev, A. Evaluating the Effectiveness of Energy-Saving Retrofit Strategies afor Residential Buildings. *Int. Rev. Civ. Eng* **2022**, *13*, 118–126. [CrossRef]
8. Ling-Chin, J.; Taylor, W.; Davidson, P.; Reay, D.; Tassou, S.; Roskilly, A.P. UK policies and industrial stakeholder perspectives on building thermal performance. *Energy Procedia* **2019**, *158*, 3375–3380. [CrossRef]
9. Barnshaw, S. The Zero Carbon and Nearly Zero Energy Standards in New Buildings. *J. Build. Surv. Apprais. Valuat.* **2018**, *6*, 344–349. Available online: https://www.ingentaconnect.com/content/hsp/jbsav/2018/00000006/00000004/art00008/supp-data (accessed on 17 December 2024). [CrossRef]
10. Juaristi, M.; Gómez-Acebo, T.; Monge-Barrio, A. Qualitative analysis of promising materials and technologies for the design and evaluation of Climate Adaptive Opaque Façades. *Build. Environ.* **2018**, *144*, 482–501. [CrossRef]
11. Zhangabay, N.; Tursunkululy, T.; Ibraimova, U.; Abdikerova, U. Energy-Efficient Adaptive Dynamic Building Facades: A Review of Their Energy Efficiency and Operating Loads. *Appl. Sci.* **2024**, *14*, 10979. [CrossRef]
12. Pelletier, K.; Wood, C.; Calautit, J.; Wu, Y. The viability of double-skin façade systems in the 21st century: A systematic review and meta-analysis of the nexus of factors affecting ventilation and thermal performance, and building integration. *Build. Environ.* **2023**, *228*, 109870. [CrossRef]
13. Pomponi, P.; Piroozfar, P.; Southall, R.; Ashton, P.; Farr, E. Energy performance of Double-Skin Façades in temperate climates: A systematic review and meta-analysis. *Renew. Sustain. Energy Rev.* **2016**, *54*, 1525–1536. [CrossRef]
14. Zhangabay, N.; Tagybayev, A.; Baidilla, I.; Sapargaliyeva, B.; Shakeshev, B.; Baibolov, L.; Duissenbekov, B.; Utelbayeva, A.; Kolesnikov, A.; Izbassar, A.; et al. Multilayer External Enclosing Wall Structures with Air Gaps or Channels. *J. Compos. Sci.* **2023**, *7*, 195. [CrossRef]
15. Santa Cruz, A.J.; Porras-Amores, C. Ventilated Façade with double chamber and flow control device. *Energy Build.* **2017**, *149*, 471–482. [CrossRef]
16. Liu, L.; Yu, Z.; Zhang, H. Simulation study of an innovative ventilated facade utilizing indoor exhaust air. *Energy Procedia* **2017**, *121*, 126–133. [CrossRef]
17. Nizovtsev, M.I.; Letushko, V.N.; Borodulin, V.Y.; Sterlyagov, A.N. Experimental studies of the thermo and humidity state of a new building facade insulation system based on panels with ventilated channels. *Energy Build* **2020**, *206*, 109607. [CrossRef]
18. Gagliano, A.; Aneli, S. Analysis of the energy performance of an Opaque Ventilated Façade under winter and summer weather conditions. *Sol. Energy* **2020**, *205*, 531–544. [CrossRef]
19. Borodulin, V.Y.; Nizovtsev, M.I. Modeling heat and moisture transfer of building facades thermally insulated by the panels with ventilated channels. *J. Build. Eng.* **2021**, *40*, 102391. [CrossRef]
20. Zhangabay, N.; Baidilla, I.; Tagybayev, A.; Sultan, B. Analysis of Thermal Resistance of Developed Energy-Saving External Enclosing Structures with Air Gaps and Horizontal Channels. *Buildings* **2023**, *13*, 356. [CrossRef]
21. Zhangabay, N.; Bonopera, M.; Baidilla, I.; Utelbayeva, A.; Tursunkululy, T. Research of Heat Tolerance and Moisture Condi-tions of New Worked-Out Face Structures with Complete Gap Spacings. *Buildings* **2023**, *13*, 2853. [CrossRef]
22. Rahiminejad, M.; Marie Pâris, A.L.; Ge, H.; Khovalyg, D. Performance of lightweight and heavyweight building walls with naturally ventilated passive and active facades. *Energy Build.* **2022**, *256*, 111751. [CrossRef]
23. Rahiminejad, M.; Khovalyg, D. Numerical and experimental study of the dynamic thermal resistance of ventilated air-spaces behind passive and active façades. *Build. Environ.* **2022**, *225*, 109616. [CrossRef]
24. Abdullah, H.K.; Faraj, S.H. Experimental study for the effect of air gap in building walls on heat gain reduction. *Mater. Today Proc.* **2021**, *61*, 1043–1051. [CrossRef]
25. Zhukov, A.D. Ventilated facade systems. *Sci. Constr. Educ.* **2016**, *1*, 1–15. Available online: https://cyberleninka.ru/article/n/sistemy-ventiliruemyh-fasadov (accessed on 17 December 2024).
26. Pirasaci, T. Investigation of phase state and heat storage form of the phase change material (PCM) layer integrated into the exterior walls of the residential-apartment during heating season. *Energy* **2020**, *207*, 118176. [CrossRef]
27. Kiryudcheva, A.E.; Shishkina, V.V. Effective Facade Systems. *Constr. Unique Build. Struct.* **2015**, *4*, 248–262. Available online: https://unistroy.spbstu.ru/userfiles/files/2015/4(31)/18_kirudcheva_31.pdf (accessed on 17 December 2024).
28. Lin, Z.; Song, Y.; Chu, Y. An experimental study of the summer and winter thermal performance of an opaque ventilated facade in cold zone of China. *Build. Environ.* **2022**, *218*, 109108. [CrossRef]
29. Zhangabay, N.; Baidilla, I.; Tagybayev, A.; Suleimenov, U.; Kurganbekov, Z.; Kambarov, M.; Kolesnikov, A.; Ibraimbayeva, G.; Abshenov, K.; Volokitina, I.; et al. Thermophysical indicators of elaborated sandwich cladding constructions with heat-reflective coverings and air gaps. *Case Stud. Constr. Mater* **2023**, *18*, e02161. [CrossRef]
30. Lykov, A.V. *Heat-and-Mass Transfer: Guide*; The Russian Energy Agency: Moscow, Russia, 1978; 479p, Available online: https://djvu.online/file/Qv0jGOssnL3dk (accessed on 15 December 2024).

31. Kutateladze, S.S. *Heat Transfer and Hydrodynamic Resistance: Reference Aid*; Energoatomizdat: Moscow, Russia, 1990; 367p. Available online: https://search.rsl.ru/ru/record/01001514242 (accessed on 18 December 2024).
32. Isachenko, V.P.; Osipova, V.A.; Sukomel, A.S. *Heat Transfer.—Textbook for Universities*, 3rd ed.; Revised and Enlarged; The Russian Energy Agency: Moscow, Russia, 1975; 488p. Available online: https://djvu.online/file/BXpZJMYm45EsC (accessed on 15 December 2024).
33. *EN 16012:2010*; Thermal Insulation for Buildings—Reflective Insulation Products—Determination of the Declared Thermal Performance. SIST: Ljubljana, Slovenia, 2010. Available online: https://cdn.standards.iteh.ai/samples/30882/98ce4dcd9c5844a3a002f2b280b61cac/SIST-EN-16012-2012.pdf (accessed on 12 January 2025).
34. Code of Rules of the Republic of Kazakhstan 2.04-01-2017. Building Climatology: State Standards in the Field of Architecture, Urban Planning and Construction. Code of Rules of the Republic of Kazakhstan.—JSC "KazNIISA", LLP "Astana Stroy-Consulting", 2017. Approved and Enacted on 20 December 2017. 43p. Available online: https://gos24.kz/uploads/documents/2022-12/sp-rk-2.04-01-2017-stroitelnaya-klimatologiya.pdf (accessed on 26 December 2024).
35. Weather Forecast. Available online: https://www.kazhydromet.kz/ru/ (accessed on 26 December 2024).
36. Code of Rules of the Republic of Kazakhstan 2.04-107-2022. Building Heat Engineering: State Standards in the Field of Architecture, Urban Planning and Construction. Code of Rules of the Republic of Kazakhstan.—JSC "KazNIISA", LLP "Astana Stroy-Consulting", 2013. Approved and Enacted on 1 July 2015. p. 80. Available online: https://online.zakon.kz/Document/?doc_id=39838250 (accessed on 26 December 2024).
37. Code of Rules of the Republic of Kazakhstan 2.04-106-2012. Designing of Thermal Protection of Buildings: State Standards in the Field of Architecture, Urban Planning and Construction. Code of Rules of the Republic of Kazakhstan.—JSC "KazNIISA", LLP "Astana Stroy-Consulting", 2013. Approved and Enacted on 1 July 2015. p. 153. Available online: https://online.zakon.kz/Document/?doc_id=35957424 (accessed on 16 December 2024).
38. Interstate Building Regulations 2.04-02-2004 Thermal Protection of Buildings. 2011, p. 48. Available online: https://online.zakon.kz/Document/?doc_id=30075061 (accessed on 16 December 2024).
39. Interstate Code of Rules 2.04-101 Design of Thermal Protection of Buildings. 2001; p. 154. Available online: https://www.arxkom.gov.az/qanunvericilik/normativler/muhendis-sistemleri/proektirovanie-teplovoy-zashchity-zdaniy (accessed on 16 December 2024).
40. Malyarenko, V.A. *Fundamentals of Thermal Physics of a Building/Textbook*; KhNAGKh: Kharkov, Ukraine, 2006; 499p. Available online: https://reallib.org/reader?file=1503517 (accessed on 16 December 2024).
41. *EN ISO 6946:2017*; Building Components and Building Elements. ISO: Geneva, Switzerland, 2017. Available online: https://www.en-standard.eu/iso-6946-2017-building-components-and-building-elements-thermal-resistance-and-thermal-transmittance-calculation-methods/ (accessed on 12 January 2025).
42. Leontyev, N.E. *Fundamentals of the Theory of Filtration*; Publishing House of CPI at the Mechanics and Mathematics Faculty of MSU: Moscow, Russia, 2009; 88p. Available online: https://gidropraktikum.narod.ru/Leontiev-2017.pdf (accessed on 16 December 2024).
43. *ISO 13788:2001*; Hygrothermal Performance of Building Components and Building Elements—Internal Surface Temperature to Avoid Critical Surface Humidity and Interstitial Condensation—Calculation Methods. ISO: Geneva, Switzerland, 2001. Available online: https://cdn.standards.iteh.ai/samples/22203/9af8a82659944443b0873c17f99960e7/ISO-13788-2001.pdf (accessed on 12 January 2025).
44. *EN 15026:2023*; Hygrothermal Performance of Building Components and Building Elements—Assessment of Moisture Transfer by Numerical Simulation. SIST: Ljubljana, Slovenia, 2023. Available online: https://standards.iteh.ai/catalog/standards/cen/65e1b928-ca9c-4a7a-ac09-7f9776e3e27b/en-15026-2023 (accessed on 12 January 2025).
45. A Patent of the Republic of Kazakhstan for the Invention—Multilayer Energy-Saving Wall Enclosing Structure with Air Layers, 2024, No. 36864. Available online: https://qazpatent.kz/ru (accessed on 17 December 2024).

Disclaimer/Publisher's Note: The statements, opinions and data contained in all publications are solely those of the individual author(s) and contributor(s) and not of MDPI and/or the editor(s). MDPI and/or the editor(s) disclaim responsibility for any injury to people or property resulting from any ideas, methods, instructions or products referred to in the content.